AD-A183 208 POST-BUCKLING DAMAGE TOLERANCE AND MANUFACTURING TECHNIQUES FOR ADVANCED.. (U) MASSACHUSETTS INST OF TECH CAMBRIDGE TECHNOLOGY LAB FOR ADVAN.. J DUGUNDJI ET AL. 1/1

UNCLASSIFIED AUG 86 TELAC-86-23 AFWAL-TR-87-4006 F/G 11/4 NL

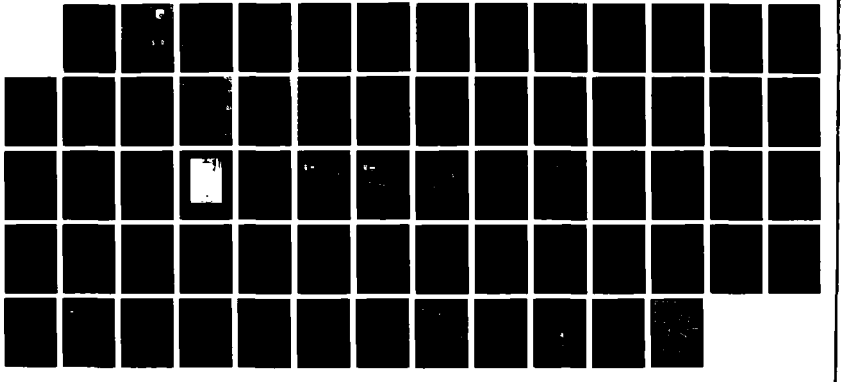

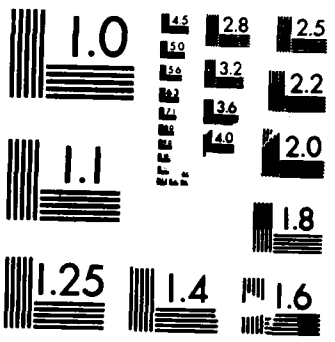

AFWAL-TR-87-4006

POST-BUCKLING, DAMAGE TOLERANCE AND MANUFACTURING TECHNIQUES FOR ADVANCED COMPOSITE MATERIALS

John Dugundji, Paul A. Lagace, James W. Mar, Theodore H.H. Pian
Massachusetts Institute of Technology
Department of Aeronautics and Astronautics
77 Massachusetts Avenue
Cambridge, Massachusetts 02139

August 1986

Final Report for Period June 1983-June 1986

MATERIALS LABORATORY
AIR FORCE WRIGHT AERONAUTICAL LABORATORIES
AIR FORCE SYSTEMS COMMAND
WRIGHT-PATTERSON AIR FORCE BASE, OHIO 45433-6533

UNCLASSIFIED

SECURITY CLASSIFICATION OF THIS PAGE A183283

REPORT DOCUMENTATION PAGE

1a. REPORT SECURITY CLASSIFICATION UNCLASSIFIED	1b. RESTRICTIVE MARKINGS
2a. SECURITY CLASSIFICATION AUTHORITY	3. DISTRIBUTION/AVAILABILITY OF REPORT APPROVED FOR PUBLIC RELEASE: DISTRIBUTION IS UNLIMINTED
2b. DECLASSIFICATION/DOWNGRADING SCHEDULE	
4. PERFORMING ORGANIZATION REPORT NUMBER(S) TELAC 86-23	5. MONITORING ORGANIZATION REPORT NUMBER(S) AFWAL-TR-87-4006
6a. NAME OF PERFORMING ORGANIZATION TECHNOLOGY LABORATORY FOR ADVANCED COMPOSITES, M.I.T. 6b. OFFICE SYMBOL (If applicable) TELAC	7a. NAME OF MONITORING ORGANIZATION MATERIALS LABORATORY (AFWAL/MLBM) A.F.WRIGHT AERONAUTICAL LABORATORIES
6c. ADDRESS (City, State and ZIP Code) MASSACHUSETTS INSTITUTE OF TECHNOLOGY ROOM 33-313, 77 MASSACHUSETTS AVENUE CAMBRIDGE, MA 02139	7b. ADDRESS (City, State and ZIP Code) WRIGHT-PATTERSON AIR FORCE BASE, OH 45433-6533
8a. NAME OF FUNDING/SPONSORING ORGANIZATION AFWAL/MLBM 8b. OFFICE SYMBOL (If applicable)	9. PROCUREMENT INSTRUMENT IDENTIFICATION NUMBER F33615-83-K-5016
8c. ADDRESS (City, State and ZIP Code) MATERIALS LABORATORY WRIGHT-PATTERSON AIR FORCE BASE, OH 45433-6533	10. SOURCE OF FUNDING NOS. PROGRAM ELEMENT NO.: 62102F PROJECT NO.: 2419 TASK NO.: 01 WORK UNIT NO.: 54
11. TITLE (Include Security Classification) POST-BUCKLING, DAMAGE TOLERANCE, AND MANUFACTURING TECHNIQUES FOR ADVANCED COMPOSITE MATERIALS	
12. PERSONAL AUTHOR(S) J. OUGUNOJI: P.A.LAGACE: J.W.MAR: T.H.H.PIAN	
13a. TYPE OF REPORT FINAL REPORT	13b. TIME COVERED FROM 6/83 TO 6/86
14. DATE OF REPORT (Yr., Mo., Day) 1986, August	15. PAGE COUNT 65
16. SUPPLEMENTARY NOTATION	

17 COSATI CODES		
FIELD	GROUP	SUB GR
13	13	

18. SUBJECT TERMS (Continue on reverse if necessary and identify by block number)
ADVANCED COMPOSITES, POST-BUCKLING, DAMAGE TOLERANCE, PRESSURIZED CYLINDERS

19. ABSTRACT (Continue on reverse if necessary and identify by block number)

This report describes a basic research program to study the post-buckling, the damage tolerance, and manufacturing techniques for various built-up, composite structures. Five separate investigations are briefly summarized here. These dealt with (1) buckling and failure studies of integrally stiffened graphite/epoxy panels, (2) finite element and experimental studies of buckling of laminated thin-wall, graphite structures, (3) damage tolerance of pressurized graphite/epoxy cylinders initiated by slits at various angles, (4) damage tolerance of pressurized graphite/epoxy cylinders flawed with slits and holes, and (5) damage tolerance of graphite/epoxy cylinders with a high strain-to-failure matrix system. These studies help provide information on the use of graphite/epoxy composites in heavily loaded structures. For more thorough descriptions and details, refer to the individual reports cited here.

20. DISTRIBUTION/AVAILABILITY OF ABSTRACT UNCLASSIFIED/UNLIMITED ☒ SAME AS RPT ☐ DTIC USERS ☐	21. ABSTRACT SECURITY CLASSIFICATION UNCLASSIFIED
22a. NAME OF RESPONSIBLE INDIVIDUAL J. WHITNEY	22b. TELEPHONE NUMBER (Include Area Code) (513)255-3068 22c. OFFICE SYMBOL AFWAL/MLBM

DD FORM 1473, 83 APR EDITION OF 1 JAN 73 IS OBSOLETE

UNCLASSIFIED

SECURITY CLASSIFICATION OF THIS PAGE

FOREWORD

The final report describes work done at the Technology Laboratory for Advanced Composites (TELAC) of the Massachusetts Institute of Technology for the Materials Laboratory, Air Force Wright Aeronautical Laboratories, under Contract No. F33615-83-K-5016. Dr. James M. Whitney was the contract monitor.

The work reported herein was performed during the period 1 June 1983 to 30 June 1986. The work represents the efforts of several graduate and undergraduate students under the direction of the indicated faculty and laboratory supporting staff.

TABLE OF CONTENTS

LIST OF FIGURES

LIST OF FIGURES (Cont'd)

LIST OF FIGURES (Cont'd)

1. INTRODUCTION

The Technology Laboratory for Advanced Composites (TELAC) of the Department of Aeronautics and Astronautics at M.I.T. has developed facilities in recent years, to examine the structural properties of advanced composite materials and the structures built from them.

The present report describes a basic research program undertaken by TELAC to study the post-buckling, the damage tolerance, and manufacturing techniques for various built-up, composite structures. The work took place over a 3-year period, and was conducted by various investigators. Five separate investigations were completed and have been more fully reported in student theses or other laboratory reports which are referenced here. These investigations dealt with (1) buckling and failure studies of integrally stiffened graphite/epoxy panels, (2) finite element and experimental studies of buckling of laminated thin-wall composite structures, (3) damage tolerance of pressurized graphite/epoxy cylinders initiated by slits at various angles, (4) damage tolerance of pressurized graphite/epoxy cylinders flawed with slits and holes, and (5) damage tolerance of pressurized graphite/epoxy cylinders with a high strain-to-failure matrix system.

A summary of the above investigations is given in the present report. For more thorough descriptions and details, refer to the individually referenced reports cited here.

2. BUCKLING STUDIES OF INTEGRALLY STIFFENED GRAPHITE/EPOXY PANELS

A series of thirteen integrally stiffened graphite/epoxy panels 13" x 12" (330 mm x 305 mm) were constructed and instrumented as shown in Figure 1. These panels were made of Hercules AS1/3501-6, and consisted of $[\pm 45/0_2]_s$ skins, with three four-ply 1" (25.4 mm) square stiffeners integrally attached to them (the bottom two skin plies wrapped around the three stiffeners). The entire panel assembly was cocured using square rubber mandrels inserted in the square tubes to preserve the shape during the cure. Subsequently, aluminum end fittings were made and embedded in epoxy to distribute the compressive load evenly along the edges. Details of the manufacturing technique for these panels can be found in Chisolm [1] and Wang [2].

The panels were placed in an MTS testing machine and loaded in compression to failure. A total of 10 strain gages, attached to the panels as shown in Figure 1, recorded the strains simultaneously during the compression tests. Buckle deformations were observed visually. Figure 2 shows a panel during testing.

Figure 3 gives the results of the compression tests on these 13 manufactured panels. Omitting panels 7 and 11, which were improperly cured or loaded, and panels 1 and 2, which were on the initial part of the manufacturing learning curve, the results indicate that with reasonable care in manufacturing quality, the present type panel can support over 16,000 lbs (71.2 KN) before failure.

Figures 4 and 5 show the strains on the plate between the stiffeners and on the stiffeners themselves, respectively for panel no. 9. The plate between the stiffeners begins to buckle at about 5,500 lbs (24.5

KN), the stiffeners themselves begin to buckle at about 13,000 lbs, and the maximum load achieved is about 17,500 lbs (77.9 KN). Also, a sudden snap-through occurred on one of the plates between the stiffeners at about 7,000 lbs (31.2 KN). The other panels showed similar behavior as panel 9, except that the snap-through was often absent.

Simple estimates were made for the onset of buckling in the plates between the stiffeners and for the maximum load carrying capacity of the panels. For these estimates, the panels were considered as consisting of three parts, namely, (A) three sides of a stiffener with two skin plies attached on the outsides, (B) the fourth side of a stiffener with the remaining six skin plies attached, and (C) the eight skin plies between (and beyond) the stiffeners. The total unwrapped width of each of these parts and the associated ply layup (for panel 9) were b_A = 9" (229 mm) with $[\pm 45/+15/0_2/+15]_T$, b_B = 3" (76.2 mm) with $[+15/0_2/+15/0_2/\pm 45]_T$, and b_c = 9" (229 mm) with $[\pm 45/0_2]_s$, respectively. Assuming the same strain ε_{11} in all three parts and using appropriate laminate stiffnesses, the total load P would be distributed into each of the three parts as,

$$P_i/P = (b/a_{11})_i / \sum_j (b/a_{11})_j \qquad (1)$$

where a_{11} is the leading element of the inverted extensional stiffness matrix $[a_{ij}] = [A_{ij}]^{-1}$ of each part i, and b is its unfolded length. This gave load distributions of $P_A/P = 0.35$, $P_B/P = 0.23$, $P_C/P = 0.42$, respectively. For the buckling of the plate between the stiffeners, clamped orthotropic plate theory [3] gives the critical buckling load per unit width, $(N_{xx})_{cr}$ as

$$(N_{xx})_{cr} = \frac{\pi^2 (D_{11} D_{22})^{1/2}}{b^2} \, k_o \qquad (2)$$

where,

$$k_o = 4.52 + 2.45\ D^*$$

$$D^* = \frac{D_{12} + 2D_{66}}{(D_{11}D_{22})^{1/2}}$$

In the above expressions, the D_{ij}'s are the plate bending stiffnesses, b is the plate width, k_o is the buckling coefficient for long panels defined by $(D_{22}/D_{11})^{1/4}$ L/b > 3, and L is the plate length. Applying this simple expression and ignoring D_{16}, D_{26} coupling terms gave $(N_{xx})_{cr}$ = 309.4 lbs/in (54,200 N/m), which with appropriate load redistrubtion, implied plate buckling at a total load P = 6,630 lbs (29.5 KN). This gave a rough estimate of the observed data in Figure 4.

For the maximum load carried by the panel, it was assumed that the stiffeners (and its attached skin) carried all the load without buckling, while the skin plies buckled and carried no load. Using a design maximum strain criterion of 4,000 μstrain, and redistributing the total load according to Equation (1) as P_A/P = 0.60, P_B/P = 0.40, resulted in a value of the failure load of P_{cr} = 22,600 lbs (100.4 KN). This again gave a rough estimate of the observed failure loads in Figure 5.

The present investigation constituted a preliminary study to show the feasibility of manufacturing and testing integrally stiffened graphite/epoxy panels. A more accurate analytic, finite element, and

experimental investigation of such panels and their components was next undertaken by Wang [2], and is described in the next section.

3. FINITE ELEMENT AND EXPERIMENTAL STUDIES OF BUCKLING IN THIN-WALL STRUCTURES

The buckling and post-buckling behavior of laminated non-complanar thin-walled structures were investigated both analytically and experimentally in detail by Wang [2]. This constituted a natural extension of the previous investigation.

Analytically, a 32-degree-of-freedom assumed stress hybrid semiLoof finite element model was developed and utilized as the analytical tool. This semiLoof element is shown in Figure 6, and has the features that only three displacement components u, v, w are utilized at the corner and mid-side nodes, while continuity of rotation with neighboring elements is maintained by normal rotations $w_{,n}$ at two points along each side. These features make it particularly convenient for use with folded structures and at corners. An optimal stress pattern for this finite element model was obtained based on a balanced stress and displacement field technique, and programs for buckling and post-buckling analyses were developed. For some standard problems and for the prediction of buckling and post-buckling behavior in channels and square tubes, the analysis gave good results. See Figures 7 and 8.

The experimental program consisted of the testing of four types of laminated, graphite/epoxy thin-wall specimens: channels, square tubes, stiffened plates and stiffened sections. All specimens had a length of 13" (330 mm) and were manufactured from Hercules AS4/3501-6 prepreg tape, using standard TELAC procedures and appropriate mandrels for the various specimens. A special jig was built for mounting the different types of specimens in the MTS te: .ig machine and loading them in

compression. In addition to 10 strain gages attached to the specimens at various locations, deflection tracker frames holding a total of four linear variable differential transducers (LVDT's) were constructed and placed next to the specimens to measure lateral deflection during the tests. The tracker frames could be slid up and down along the specimen's axial direction to give a complete sweep of the deflection. All manufacturing and test procedures are described in detail by Wang [2].

Figure 9 gives a summary of the onset of buckling loads for the overall test program, along with the analytic predictions from the finite element method. Good agreement between experiment and theory was found for the channels and square tubes. Figure 10 gives a summary of the actual failure loads for these specimens. It should be noted that for the square tubes, the largest initial buckling load did not correspond to the largest failure load of the specimen. The channels and square tubes failed by ply delamination at the corners due to stress concentrations and large out-of-plane deflection, while the failure of the stiffened plates and stiffened sections were first caused by delamination of the base-plate from the square tube core of the stiffeners and covering face-sheet, and finally completed by ply delamination at the stiffener corners.

Figure 11 shows the strains on the stiffened panels at various indicated locations and clearly indicates the onset of buckling for the plate and the stiffener. Figure 12 shows the deflection at four points across the center of the panel. More detailed observation of the deflection patterns along the entire axial length of the panel at various loads, are shown in Figures 13 and 14. It should be noted that the stiffened panels here have a slightly smaller overall width (11" (279 mm) rather than the 12" (305 mm) of the previous investigation) and

the stiffeners are now six-ply, $[\pm 15/0]_s$ rather than the previous four-ply configuration $[+15/0]_s$. Five half waves of deflection occur for both the stiffeners and the plate between the stiffeners, indicating an interaction between the buckling of the two components. Comparison of the results of the stiffened panel with those of the stiffened section of the same panel indicated that the stiffened panel can be characterized by the behavior of its cutout part, assuming the stiffness of the stiffener is much higher than that of the skin plate.

More detailed results and conclusions from this analytical and experimental analysis of buckling of laminated thin-wall structures can be found in the report by Wang [2]. A paper based on the analytical semiLoof finite element developed here was given by Wang and Pian [4], while a subsequent paper describing the experimental results and correlations is in preparation: Wang, Pian, Dugundji and Lagace [5].

DAMAGE TOLERANCE OF PRESSURIZED GRAPHITE/EPOXY CYLINDERS INITIATED BY SLITS AT ANGLES

An investigation was made into the damage tolerance and astrophic failure of pressurized graphite/epoxy cylinders initiated by ll flaws in the walls. This work followed on previous investigations at LAC by Rogers [6] and Graves [7], and is reported more fully by Chang Mar [8], [9].

For this investigation, a series of eight graphite/epoxy cylinders e constructed and tested, to obtain the internal pressure required to se rapid fracture to initiate by through-the-thickness slits at various les. The cylinders were made from Hercules A370-5H/3501-6 phite/epoxy five-harness weave cloth prepreg, in a $(0, 45)_s$ layup rantheses are used here in place of square brackets to indicate fabric s, and the angle represents the warp direction of a ply weave). The nders had a diameter of 12" (305 mm), a length of 24" (610 mm), and e fitted with end caps. Slits of varying length were cut through the thickness at different angles to the longitudinal axis, and sealed with hes made of thin aluminum strips. See Figure 15 for overall layout details.

Testing took place in a large blast chamber capable of absorbing the rgy from the explosion of 2 pounds of TNT. Internal pressure in the nder was increased monotonically until catastrophic failure was ated at the slits. Internal pressure and strains at various locations e measured during the test. The failure itself was quite violent, and important part of the test procedure was in retrieving the pieces of failed cylinder so that fracture paths could be determined.

Figure 16 gives a summary of the cylinders tested, their slit lengths and orientation, and the pressures which caused catastrophic failure. A sketch of the failure mode for a cylinder with a 45-degree slit is shown in Figure 17. Experimental failure pressures for cylinders with different length slits at a 45-degree angle are shown in Figure 18 along with some analytical predictions.

Analytic predictions for the cylinder failures were based on test data obtained on unidirectional loaded flat coupon specimens of the same layup. The flat coupon specimens were "flawed" with slits on holes and were found to reasonably fit the Mar-Lin relationship,

$$\sigma_{plate} = H_c(2a)^{-.28} \qquad (3)$$

where σ_{plate} is the far-field fracture stress for the flat coupons, H_c is the *composite fracture parameter, and (2a) is the slit length or hole diameter.* The above flat coupon relation was modified using the Folias correction [10], to account for the increased stress intensity which accompanies the localized bending of the shell wall due to the presence of a crack. A further correction using the notion of an "equivalent" cylinder, was used to extend the prediction to account for the angle of the slit. This involved determining the local radii of curvature perpendicular and parallel to the slit, to obtain an equivalent stress concentration factor K for the specimen. The prediction for failure stress σ_f of the cylinders were then expressed as,

$$\sigma_f = \sigma_{plate} K \qquad (4)$$

where σ_{plate} is the stress from the Mar-Lin relation, Equation (3). Analytic predictions based on this method are shown in Figure 18 for the

45-degree slits. Figure 19 shows another way of depicting the results, namely, the slit length required to cause rapid fracture at an internal pressure of 1 MPa versus the angle of the slit. (The experimental data for this latter plot were adjusted somewhat to bring them to 1 MPa levels.)

Generally, comparison of predicted values with experimental results for these pressurized cylinders with slits at angles, showed the failure estimation method is reasonable. It is noted that initial paths of the fractures ran both longitudinally and circumferentially from the ends of the angled slits, rather than along the angle of the slit (see Figure 17). More detailed results and conclusions from this study can be found in the report by Chang and Mar [8], and in a published article, Chang and Mar [9]. Also, a general paper on fracture, longevity, and damage tolerance of graphite/epoxy composite structures by Mar [11], makes use in part of some of these results.

5. DAMAGE TOLERANCE OF PRESSURIZED GRAPHITE/EPOXY CYLINDERS FLAWED WITH SLITS AND HOLES

Following on the previous study of damage tolerance and catastrophic failure of pressurized graphite/epoxy cylinders with slits at angles, an investigation was undertaken of the effects of different types of flaws on the failure mechanisms of these cylinders. The flaws included (a) two colinear longitudinal slits, (b) circular holes, (c) elongated (long) holes, and (d) slits emanating from holes. This work, which is briefly described here, is reported more fully in a report by Chang and Mar [12].

For this investigation, a series of 15 graphite/epoxy cylinders were constructed and tested, as in the previous investigation, to obtain the internal pressure required to cause catastrophic failure for the given size and shape of flaw. The cylinders were all of the same material and dimensions as before, only the flaw was now different. Figures 20 through 23 give a summary of the specific cylinders tested, the flaw type and size, and the pressures for catastrophic failure. Sketches of typical failure modes for each of the four types of flaws are given in Figures 24 through 27. All fracture paths seem to run longitudinally from the flaw until they bifurcate near the ends of the cylinder. Occasionally, a fracture would run circumferentially, but this was usually after the longitudinal path was established. Figure 28 gives typical results from strain gages oriented circumferentially and located axially at 10, 30, 80 and 160 mm from the edge of the hole, for a cylinder with a hole. The higher strain state near the hole is apparent.

Analytical predictions of the failure pressures for the various flaw types were again based on the Mar-Lin relationship with suitable

modifications for the localized shell bending, and the flaw shape. The predictions for failure stress σ_f were again expressed as

$$\sigma_f = \sigma_{plate}/K \tag{4}$$

where σ_{plate} is the stress from the flat plate Mar-Lin relation, Equation (3), and K is a stress concentration factor for the particular flaw which involves mainly the shell parameter,

$$\lambda = [12(1-\nu^2)]^{1/4}\, a/\sqrt{Rh} \tag{5}$$

In the above, R, h, a, are the shell radius, shell thickness, and flaw semi-length (i.e., radius) respectively. Although for flat plate tests, holes and slits of the same size lead to the same fracture stress, for cylinders the slits seem to be more critical above a value of $\lambda = 3.7$ for the cylinders (Figure 29) due to the localized bending at the tip of the slit.

Generally again, comparison of predictions with the experimental test results showed that the method is reasonable for estimating failure. More detailed results and conclusions can be found in the report by Chang and Mar [12].

6. DAMAGE TOLERANCE OF PRESSURIZED COMPOSITE CYLINDERS WITH A HIGH STRAIN-TO-FAILURE MATRIX SYSTEM

Continuing with the study of damage tolerance of pressurized cylinders, an experimental and analytical investigation was conducted to examine the damage tolerance of graphite/epoxy cylinders and flat coupons which utilize a high strain-to-failure matrix system. The material system selected was a five-harness weave cloth prepreg, made of Hercules AS4 fiber embedded with American Cyanamid CYCOM 907 epoxy (formerly BP-907). The results were then compared with the previous investigations involving the 3501-6 epoxy matrix system. This work, which is briefly described here, is reported in detail by Saeger [13].

For this investigation, tensile tests were first run on a series of flat coupons made of the AS4/CYCOM 907 cloth fabric in $(0)_4$, $(90)_4$, $(\pm 45)_s$, and $(0, 45)_s$ layups to obtain the basic stiffness and strength properties of the material (parantheses are used here in place of square brackets to indicate fabric plies, and the angle represents the warp direction of a ply weave). A total of 65 flat coupons were tested which included unnotched specimens and specimens with different size transverse slits and holes. Figures 30 and 31 show the unnotched and notched fracture characteristics of the $(0, 45)_s$ laminate coupons with transverse slits and with holes, respectively. Each point represents the average of five tests. For these two notch shapes (transverse slits and holes), no dependence on differing notch geometry was found for the fracture stress, and the fracture stresses seemed to correlate reasonably with the Mar-Lin theory as well as the Whitney-Nuismer average stress and point stress criteria.

Internal pressure tests were than run on a series of 5 cylinder specimens made of the same AS4/CYCOM 907 material with a four-ply

$(0, 45)_s$ layup. The cylinders had the same dimensions as in previous tests, i.e., 610 mm long with a diameter of 305 mm, and were cut through with axial slits of 50, 75, 100, and 150 mm lengths, and pressurized monotonically to failure. Strain gages were placed at a number of locations along the extension of the slit to measure circumferential strain. Figure 32 shows the measured strains at five locations during pressurization of a cylinder with a 75-mm slit. The large strains close to the slit are to be noted. Figure 33 indicates the failure pressure obtained for a given size slit.

To relate the flat coupon fracture data to the pressurized cylinder failure, account should be taken of the localized stress intensification near the slit (crack) tip due to the cylinder's bending action there. Rather than using the Folias correction [10] as in the previous investigations, it was decided here to solve the problem numerically in order to get a better understanding of the stress state near the slit. Accordingly, a finite difference solution was undertaken to solve the shallow shell equations,

$$\frac{Eha^2}{R}\frac{\partial^2 w}{\partial x^2} + \nabla^4 F = 0$$

$$\nabla^4 w - \frac{a^2}{RD}\frac{\partial^2 F}{\partial x^2} = -\frac{p_o a^4}{D} \qquad (6)$$

in the neighborhood of the slit tip. In the above, E and D are the modulus of elasticity and bending stiffness of the quasi-isotropic $(0, 45)_s$ laminate, R is the cylinder radius, h the thickness, p_o the pressure, and the coordinates x and y are nondimensionalized with respect to the half-slit

length, a. A refined finite difference grid for the analysis is shown in Figure 34, which was solved after a coarser grid was solved. Figure 35 shows the resulting displacements w near a 75-mm slit, while Figure 36 gives a contour plot of the resulting hoop stress concentration factors $K = \sigma_{yy}/\sigma_{hoop}$ in that vicinity. The corresponding hoop strains measured during the tests are compared with the analysis in Figure 37. Reasonable agreement between test and analysis is obtained, showing the large strain concentration factors developed, and the extent of the edge zone in which they arise. Similar agreement was obtained for the other slit lengths.

Estimates were made of the failure pressures of the cylinders with slits by correcting the flat plate coupon data for the stress intensification effects due to the cylindrical geometry. The Whitney-Nuismer average stress criterion, together with results from the finite difference analysis, gave good correlation with the experiments, as seen in Figure 33. Also shown is the Mar-Lin criterion corrected by the simple Folias correction described in the previous sections. The agreement here, although adequate, was not as good as for the Whitney-Nuismer criterion.

Comparison of the above tests on high strain-to-failure CYCOM 907 epoxy with earlier tests on 3501-6 epoxy seemed to indicate that, both from the coupon tests and from the cylinder tests, the "tough" CYCOM 907 matrix system was more notch sensitive than the baseline 3501-6 epoxy system, and hence, may not always be desirable. For more details of the present investigation, refer to Saeger [13]. A paper based on this work is currently in preparation [14].

7. CONCLUDING REMARKS

The present report described a basic research program to study the post-buckling, damage tolerance, and manufacturing techniques for some heavily loaded, built-up graphite/epoxy composite structures. Channels, square tubes, and integrally stiffened panels were built, analyzed, and tested. The nature of the buckling and failure modes were noted. An analysis utilizing a stress hybrid semiLoof finite element was developed and used to describe the behavior of these folded structures. Also, a series of pressurized cylinders (representing pressurized fuselages) were built, analyzed, and tested to determine the damage tolerance and failure modes due to various type flaws. Simple prediction methods using the Folias stress intensification factor were used to predict failure. The use of a high strain-to-failure matrix system resulted in greater notch sensitivity.

The study reported helps provide some additional information on the use of graphite/epoxy composites in heavily loaded structures. For more thorough description and details, refer to the individual reports cited here.

REFERENCES

1. Chisolm, J., "Graphite Epoxy Plates with Stiffeners: Manufacture and Compressive Testing," TELAC Report 83-10, Massachusetts Institute of Technology, May 1983.

2. Wang, Cheng, "Finite Element and Experimental Studies of Buckling of Laminated Thin-Wall Structures," Sc.D. Thesis, Department of Aeronautics and Astronautics, Massachusetts Institute of Technology, May 1985, also, TELAC Report 86-19, M.I.T., May 1986.

3. Brunelle, E.J., and Oyibo, G.A., "Generic Buckling Curves for Specially Orthotropic Rectangular Plates," AIAA Journal, Vol. 21, No. 8, August 1983, pp. 1150-1156.

4. Wang, C. and Pian, T.H.H., "Hybrid SemiLoof Element for Buckling of Thin-Walled Structures," papers submitted to the International Conference on Computational Engineering Mechanics, Beijing, China, June 21-25, 1987.

5. Wang, C., Pian, T.H.H., Dugundji, J., and Lagace, P.A., "Analytic and Experimental Studies on the Buckling of Laminated Thin-Wall Structures," paper submitted to the 28th AIAA/ASME/ASCE/AHE Structures, Structural Dynamics and Materials Meeting, Monterey, CA, April 6-8, 1987.

6. Rogers, J.C., "An Investigation of the Damage Tolerance Characteristics of Graphite/Epoxy Pressure Vessels," M.S. Thesis, Department of Aeronautics and Astronautics, Massachusetts Institute of Technology, September 1981, also, TELAC Report 81-12, M.I.T., September 1981.

7. Graves, M.J., "The Catastrophic Failure of Pressurized Graphite/Epoxy Cylinders," Ph.D. Thesis, Department of Aeronautics and Astronauatics, Massachusetts Institute of Technology, September 1982, also, TELAC Report 82-10, M.I.T., September 1982.

8. Chang, S.G., and Mar, J.W., "The Catastrophic Failure of Pressurized Graphite/Epoxy Cylinders Initiated by Slits at Various Angles," Air Force Wright Aeronautical Laboratories

Report AFWAL TR85-4056, May, 1985, also TELAC Report 84-13, M.I.T., August 1984.

9. Chang, S.G., and Mar, J.W., "The Catastrophic Failure of Pressurized Graphite/Epoxy Cylinders Initiated by Slits at Various Angles," 25th AIAA/ASME/ASCE/AHS Structures, Structural Dynamics and Materials Conference, Palm Springs, California, May 14-16, 1984, pp. 123-129.

10. Folias, E.S., "On the Prediction of Catastrophic Failures in Pressurized Vessels," Prospects of Fracture Mechanics, Edited by G.C. Sih, H.C. van Elst and D. Broek, Nordhoff International Publishing, Leyden, 1974, pp. 405-418.

11. Mar, J.W., "Fracture, Longevity, and Damage Tolerance of Graphite/Epoxy Filamentary Material," J. of Aircraft, Vol. 21, No. 1, January 1984, pp. 77-83.

12. Mar, J.W., and Chang, S.G., "The Catastrophic Failure of Pressurized Graphite/Epoxy Cylinders Flawed with Slits and Holes," TELAC Report 85-4, Massachusetts Institute of Technology, March 1985,

13. Saeger, K.J., "Damage Tolerance of Composite Cylinders with a High Strain-to-Failure Matrix System," Thesis, Department of Aeronautics and Astronautics, Massachusetts Institute of Technology, also TELAC Report 86-11, M.I.T., May, 1986.

14. Saeger, K.J. and Lagace P.A., "Fracture of Pressurized Composite Cylinders with a High Strain-to-Failure Matrix System," to be presented at Symposium on Composite Materials: Fatigue and Fracture (2nd Symposium) Cincinnati, Ohio, April 1987.

NOMENCLATURE

a	flaw semi-length
a_{11}	leading element of inverted extensional stiffness matrix
A_{ij}	element of extensional stiffness matrix
b	plate width
D_{ij}	element of bending stiffness matrix
D^*	bending stiffness ratio defined in Eq. (2)
E	modulus of elasticity
F	plane stress function
h	plate thickness
H_c	composite fracture parameter
k_o	plate buckling coefficient
K	stress concentration factor
L	plate length
N_{xx}	stress resultant
p_o	pressure loading
P	compressive load
R	cylinder radius
w	plate lateral deflection
ε_{11}	axial strain

λ	cylinder shell parameter defined by Eq. (5)
σ_f	fracture stress
σ_{plate}	fracture stress for flat plate
σ_{yy}	hoop stress

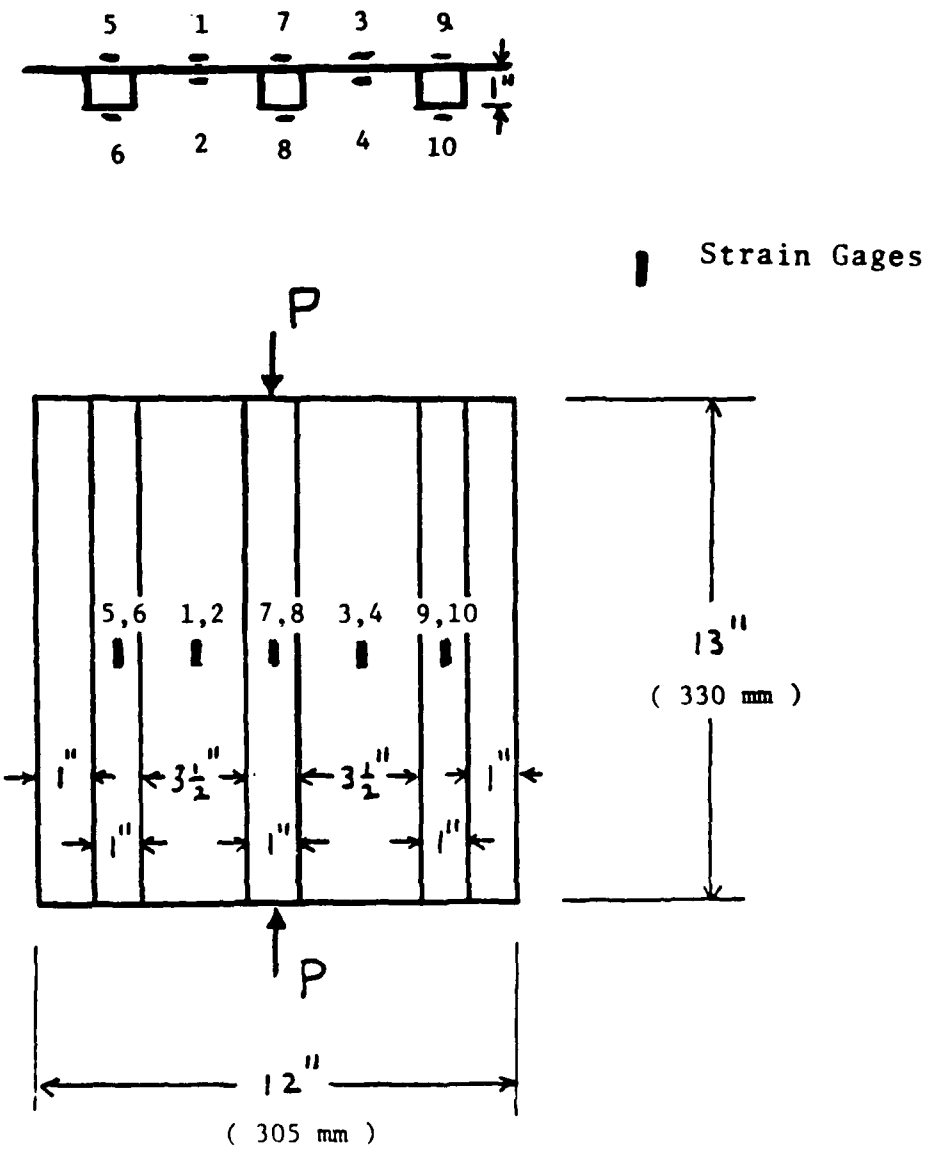

FIGURE 1 Geometry and Layout of Stiffened Panels

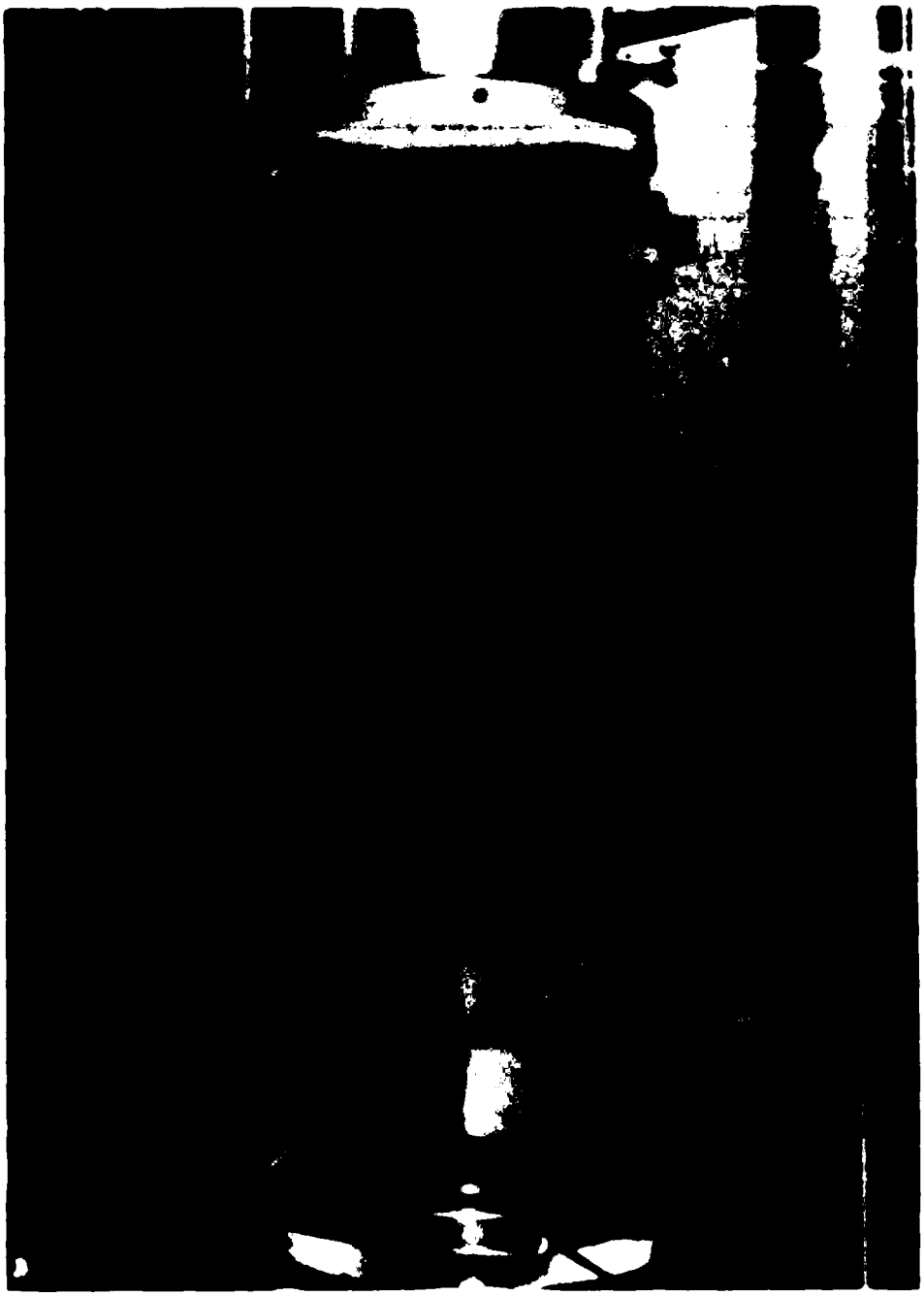

FIGURE 2 Stiffened Panel during a Compression Test

Panel	Plate Lay-up	Stiffener Lay-up	Number of Strain Gages	Maximum Load (lbs.)
1	$[\pm 45/0_2]_s$	$[\pm 45]_s$	5	13,600
2	"	"	5	13,970
3	"	"	-	Not Tested
4	"	"	10	20,100
5	"	"	10	18,100
6	"	"	-	Not Tested
7	"	"	10	11,050**
8	"	"	10	18,650
9	"	$[+15/0]_s$	10	17,700
10	"	"	10	16,050
11	"	$[\pm 30]_s$	10	12,532*
12	"	$[+15/0]_s$	10	16,250
13	"	$[0/-15]_s$	10	16,900

*Misaligned panel, fast loading
**Improper cure

FIGURE 3 Panels Manufactured and Tested

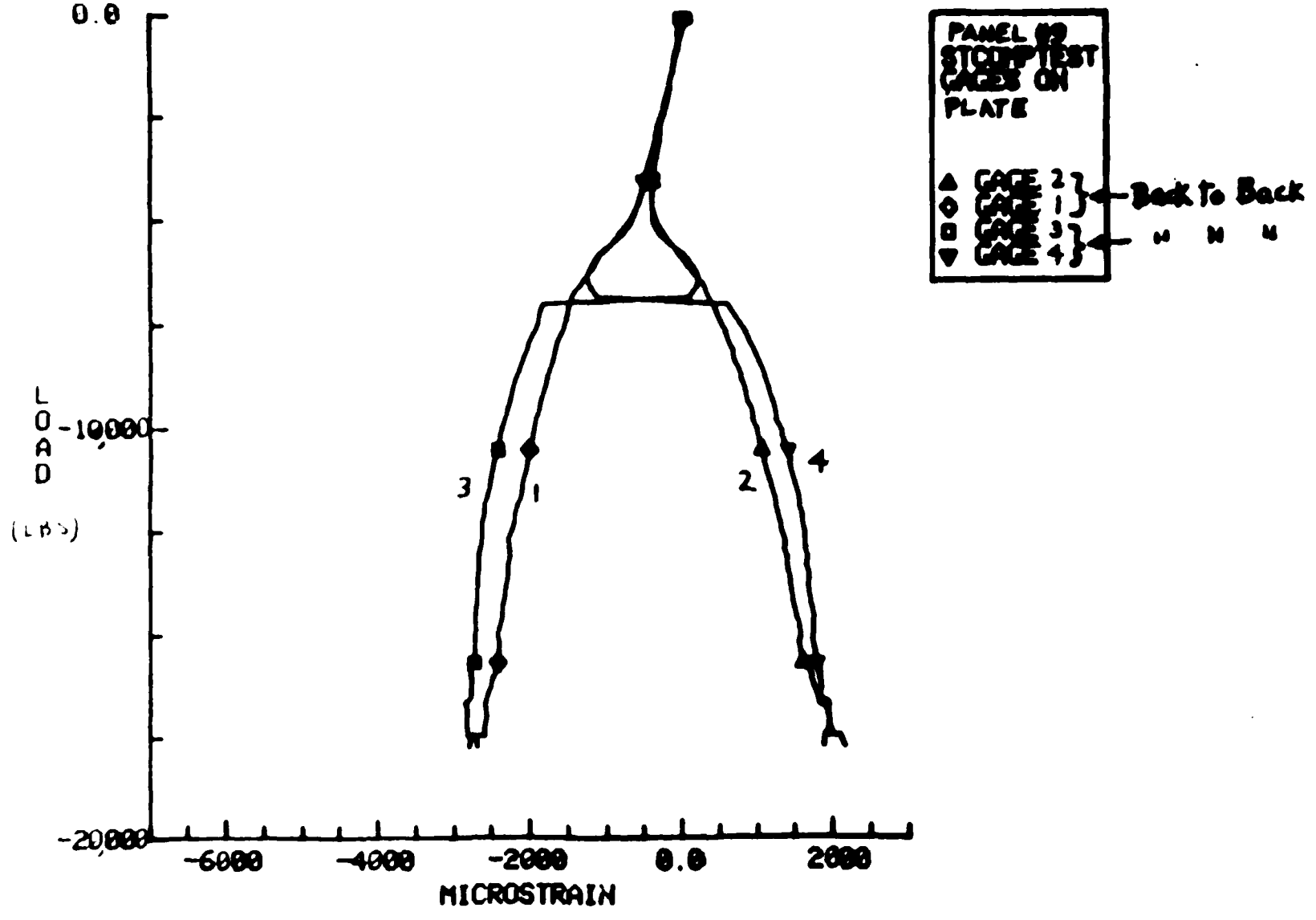

FIGURE 4 Measured Strains in Plate between Stiffners, Panel 9

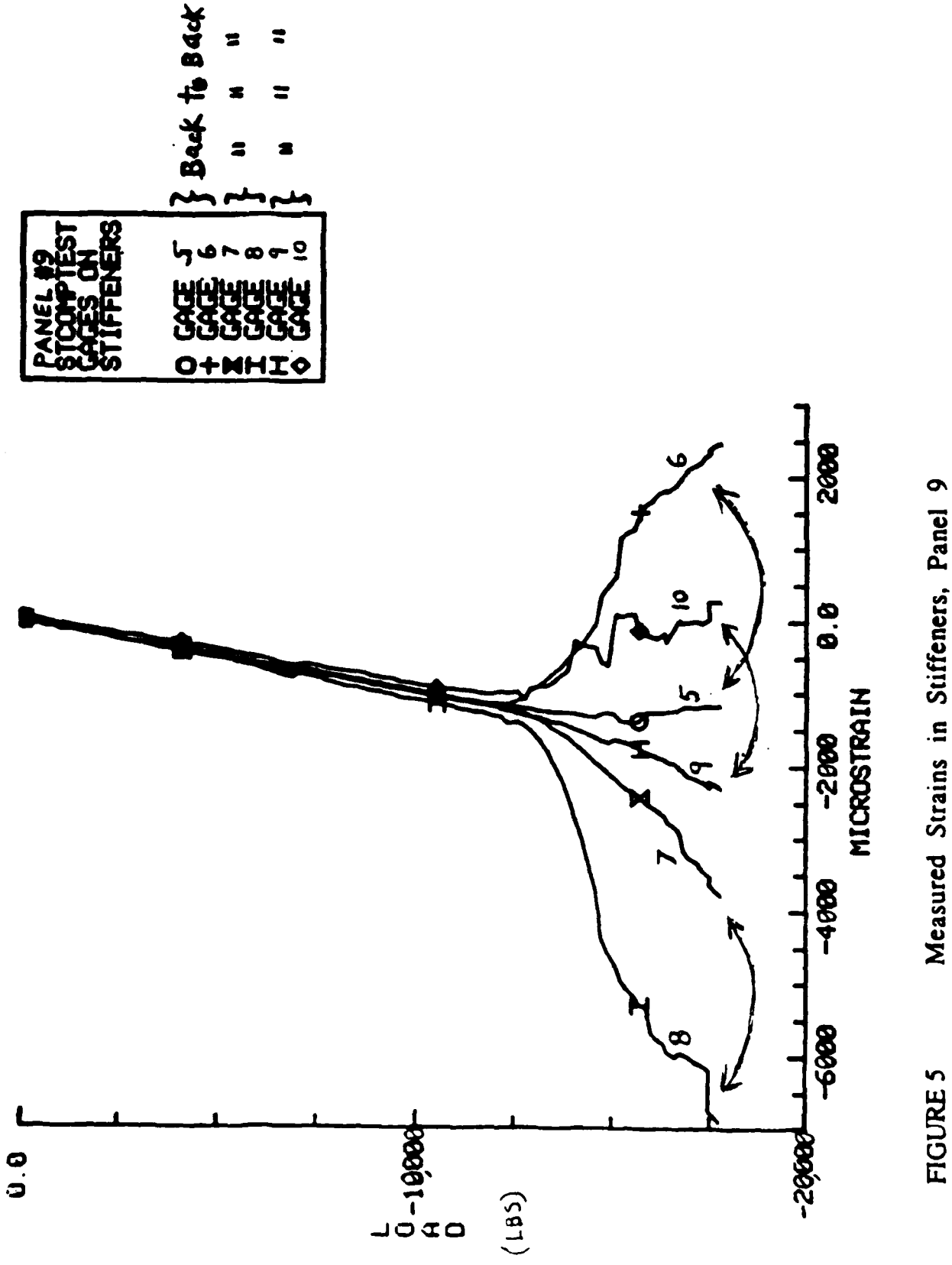

FIGURE 5 Measured Strains in Stiffeners, Panel 9

FIGURE 5 Measured Strains in Stiffeners, Panel 9

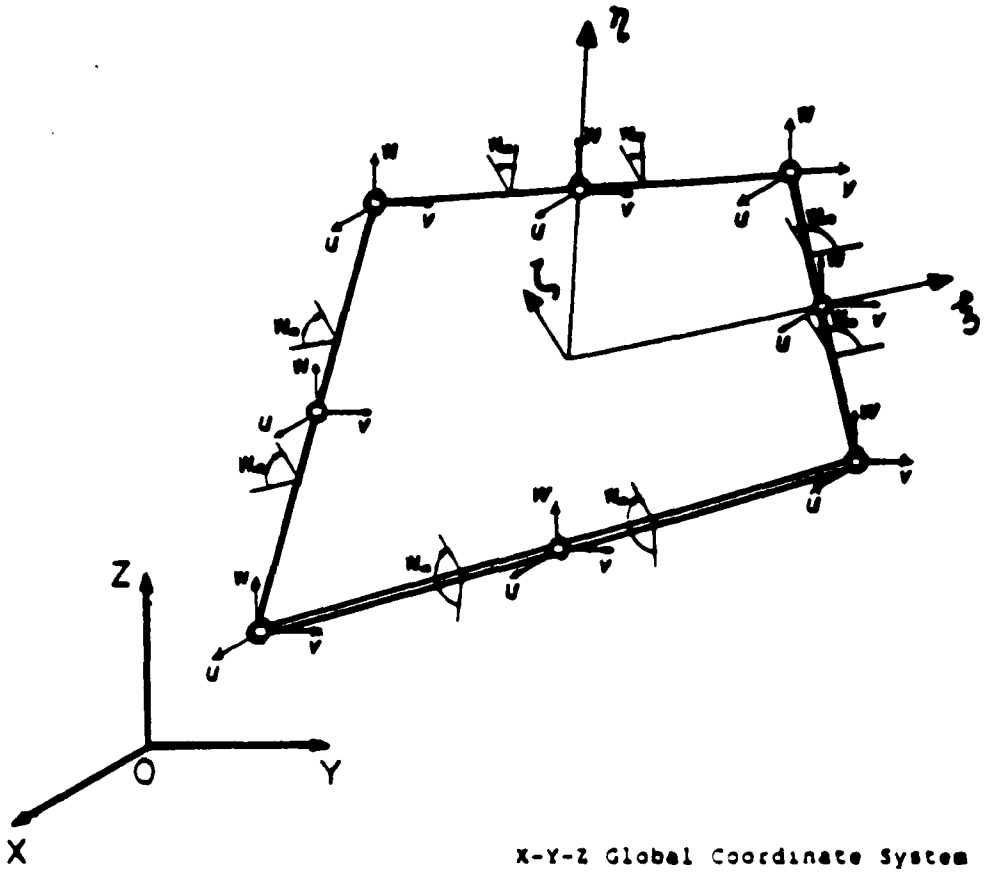

FIGURE 6 Sketch of 32 DOF SemiLoof Element Model

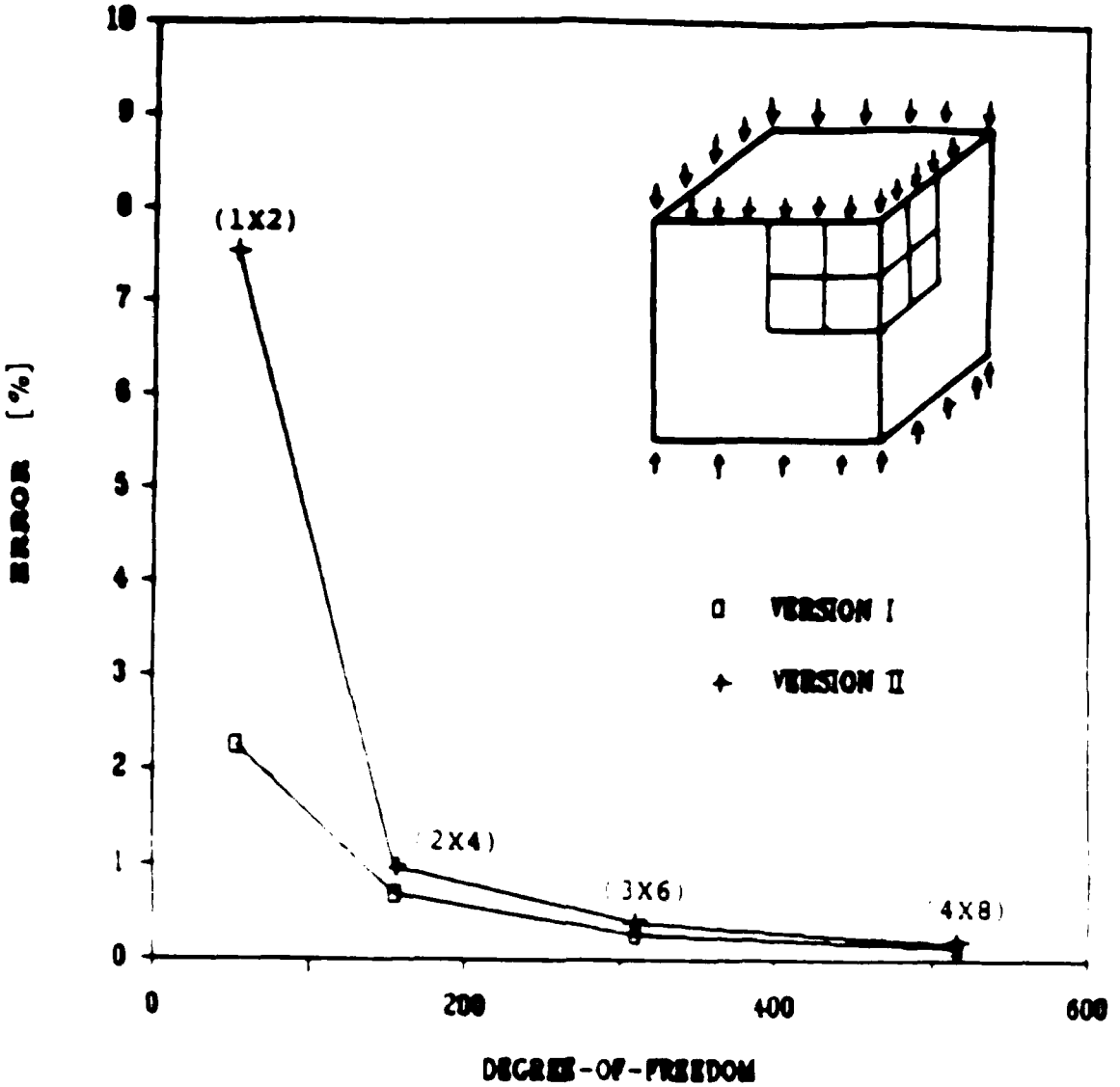

FIGURE 7 Accuracy of Buckling Load for an Isotropic, Simply Supported, Square Tube

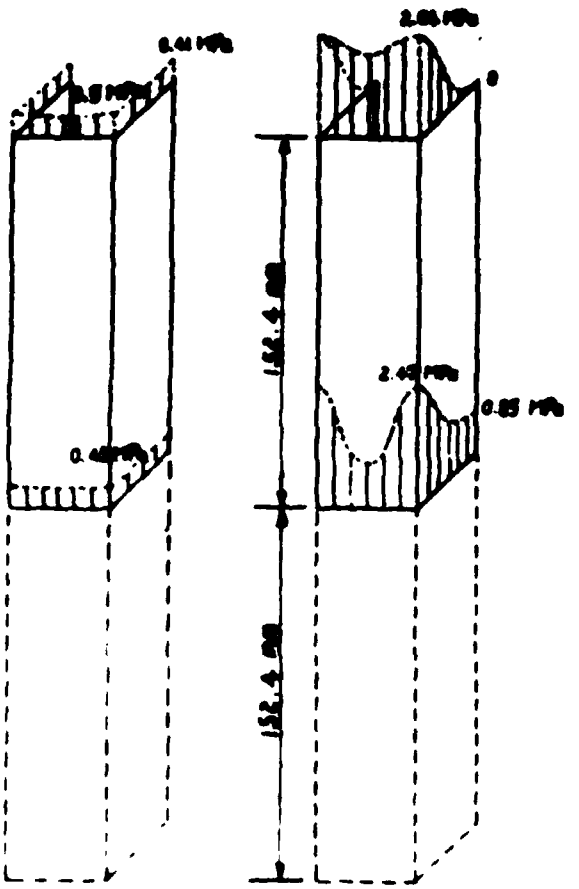

Load Level

1. P = 8.96 kN
   (buckling buckling)

2. P = 25.12 kN
   (in postbuckling range)

(1) (2)

FIGURE 8 Predicted In-Plane Longitudinal Stress Resultant Distribution

Type of Specimen	Layup	#	Experimental Result[kN]		Predict Value [kN]	Error[a]
			VALUE	MEAN (C.V.)		
CHANNEL	$[\pm 15/0]_s 2$	1 2 3	10.20 9.27 9.12	9.53 (5.03%)	9.16	4.04%
	$[\pm 15/0]_s$	1 2 3	8.08 6.67 9.75	8.17 (15.42%)	8.59	-4.89%
SQUARE SECTION	$[\pm 15/0]_{2T}$	1 2 3	6.86 9.15 8.03	8.01 (11.67%)	7.74	3.49%
TUBES	$[\pm 15_2/0_2]_T$	1 2 3	6.10 8.30 7.98	7.46 (13.01%)	6.87	8.59%
	$[\pm 45/(\pm 15)_s]_T$	1 2 3	6.73 8.94 10.75	8.81 (18.67%)	10.91	19.25%
STIFFENED PLATE[b] (skin plate buckling)	Skin Plate $[\pm 45/0_2]_s$ Tube core $[\pm 15/0]_s$	1 2 3	60.59 66.72 65.39	64.23 (4.10%)		
STIFFENED PLATE[b] (stiffener buckling)	Skin Plate $[\pm 45/0_2]_s$ Tube core $[\pm 15/0]_s$	1 2 3	100.17 114.41 100.09	104.89 (6.42%)		
STIFFENED SECTION	Same as stiffened plate layup	1 2 3	25.58 33.73 37.01	32.11 (14.97%)		

[a] The standard value to define the error is the analytical prediction.

[b] The buckling load of stiffened plates has two values: one defines the buckling load found from the bifurcation point of skin plate and another is that from the stiffeners.

FIGURE 9 Summary Data of Buckling Loads

Specimen			Experimental Results		
Type	Layup	#	Failure Load [kN]	Mean [kN]	C.V.
CHANNEL	$[\pm 15/0]_s 2$	1 2 3	29.58 29.40 31.58	30.19	3.27%
	$[\pm 15/0]_s$	1 2 3	16.17 15.44 15.04	15.55	3.01%
SQUARE SECTION	$[\pm 15/0]_{2T}$	1 2 3	14.72 15.21 13.43	14.45	5.19%
TUBE	$[\pm 15_2/0_2]_T$	1 2 3	11.78 12.86 11.92	12.19	3.94%
	$[\pm 45/(\pm 15)_s]_T$	1 2 3	11.16 13.57 13.43	12.72	8.68%
STIFFENED PLATE	Skin Plate $[\pm 45/0_2]_s$ Tube core $[\pm 15/0]_s$	1 2 3	145.01 131.89 109.87	128.92	11.25%
STIFFENED SECTION	same as panel layup	1 2 3	32.07 43.33 42.93	39.44	13.25%

FIGURE 10 Summary Data of Failure Loads

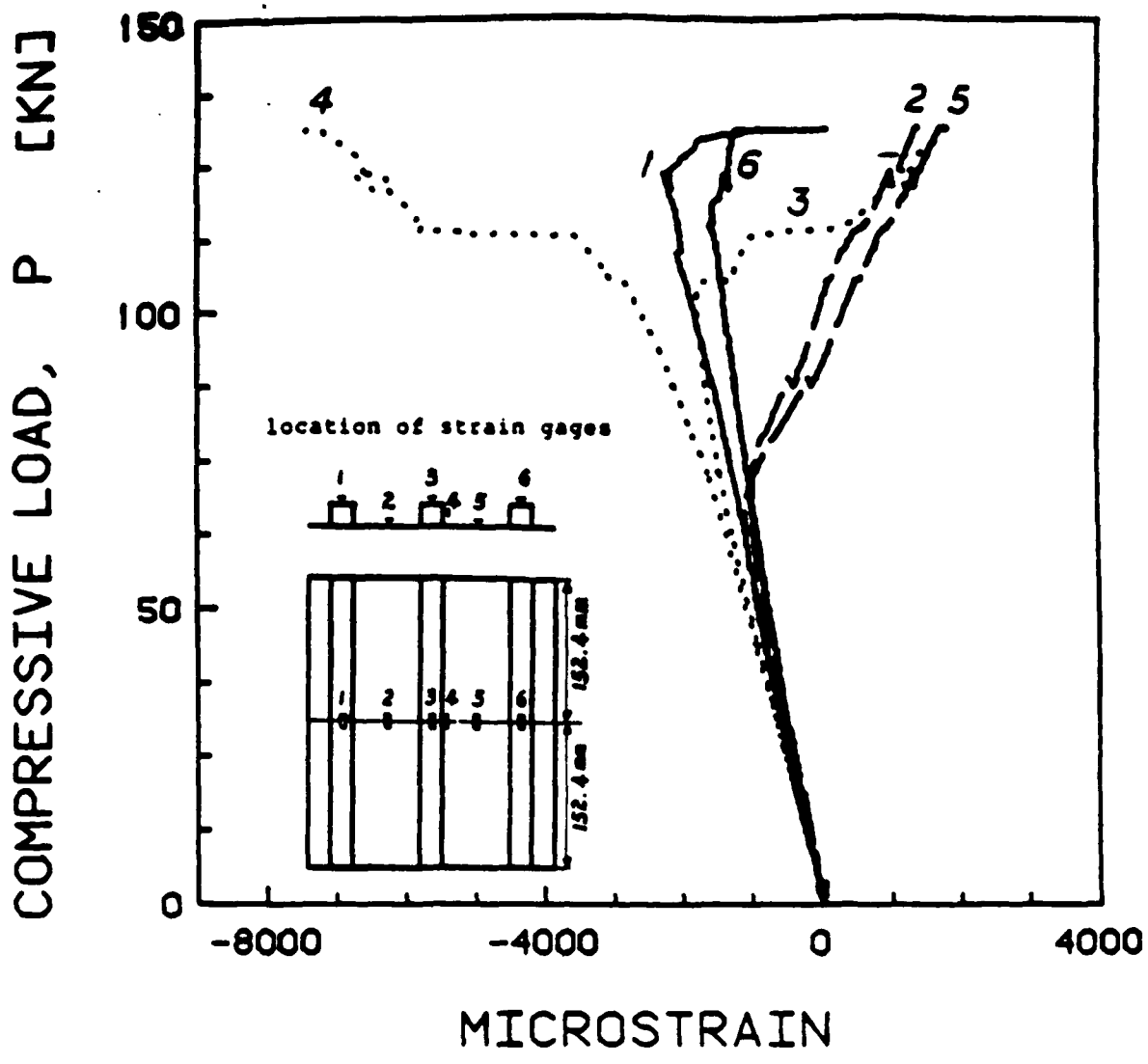

FIGURE 11 Measured Strains in Stiffened Panels at Six Locations

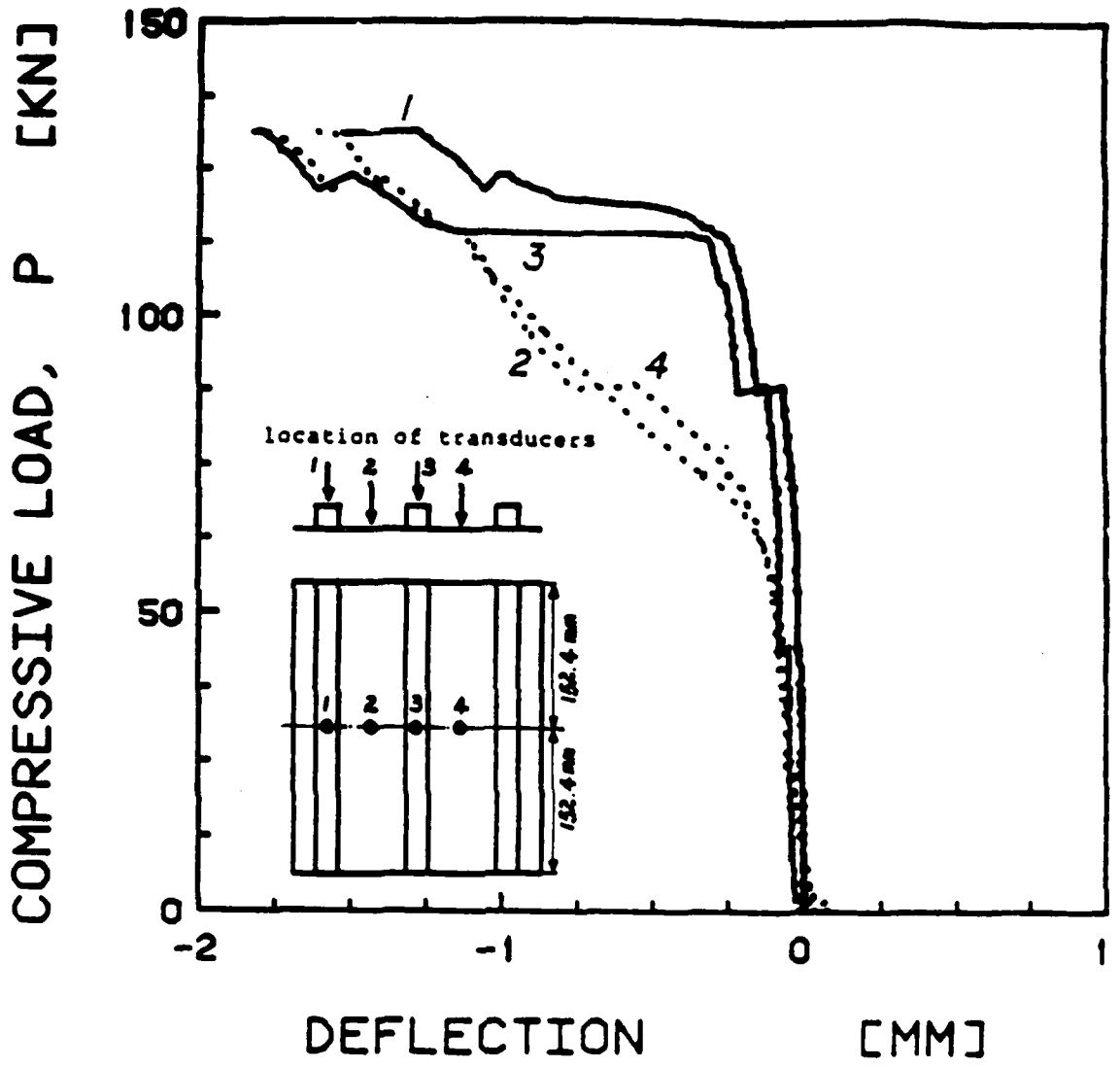

FIGURE 12 Measured Deflections of Stiffened Panels at Four Locations

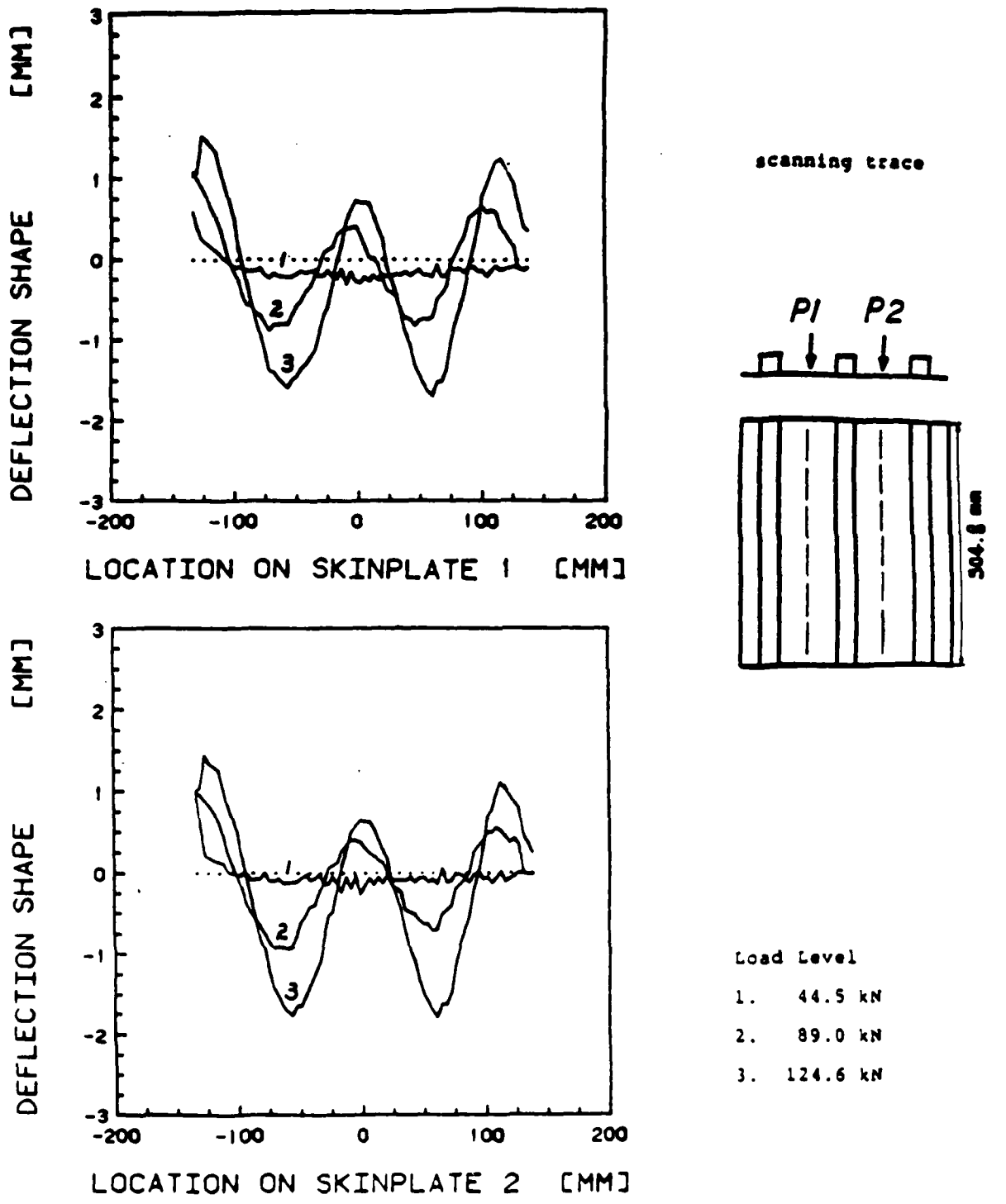

FIGURE 13 Measured Deflection Mode Shapes for Plate between Stiffners

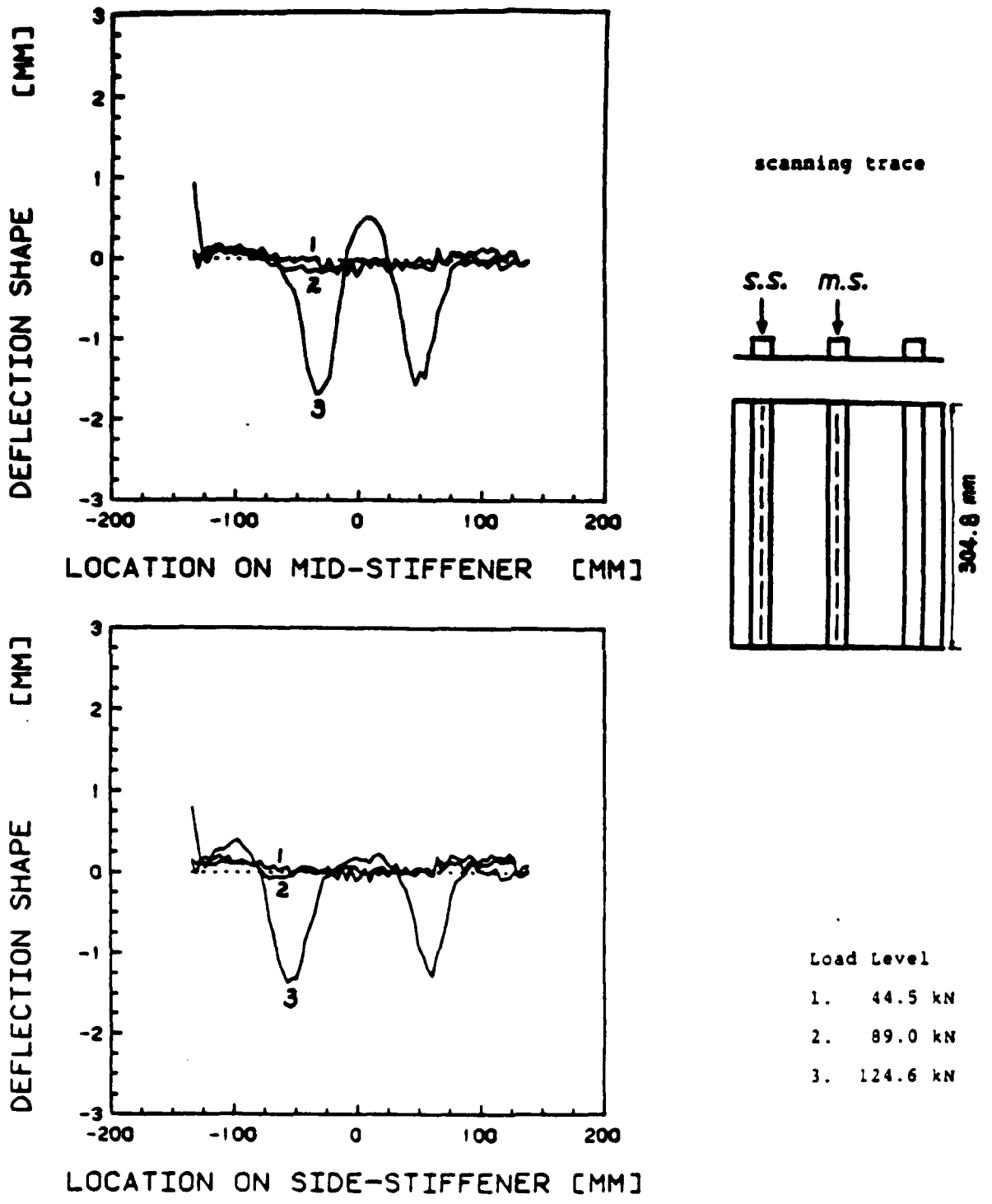

FIGURE 14 Measured Deflection Mode Shapes for Stiffeners

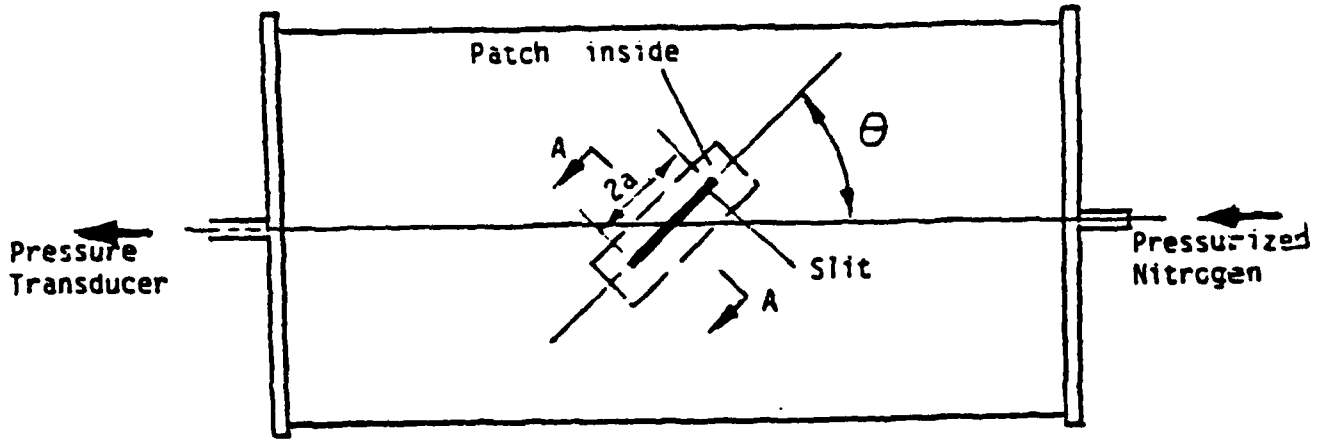

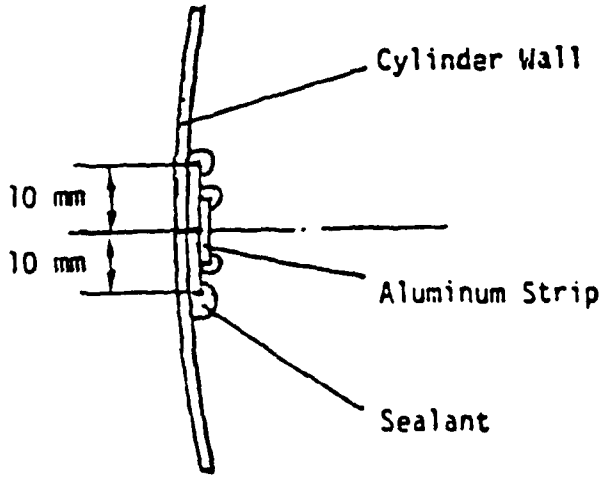

AA Section

FIGURE 15 Pressurized Cylinder Layout and Patch Details

No.	Tube No.	θ (degree)	2a (mm)	P_{fail} (MPa)	P_{cal} (MPa)	ϵ^{*}_{hoop}
1	105	0	50.8	1.001	1.144	0.00177 *
2	111	22.5	76.2	0.841	0.821	0.00148
3	110	45	63.5	1.207	1.433	0.00213
4	109	45	69.85	1.055	1.283	0.00186
5	106	45	76.2	0.931	1.166	0.00164
6	107	45	82.55	0.896	1.061	0.00158
7	108	45	88.9	0.944	0.970	0.00167
8	112	67.5	101.6	1.650	1.438	0.00292

* ϵ_{hoop} is hoop strain calculated at failure pressure.

FIGURE 16 Summary Data of Cylinders Tested

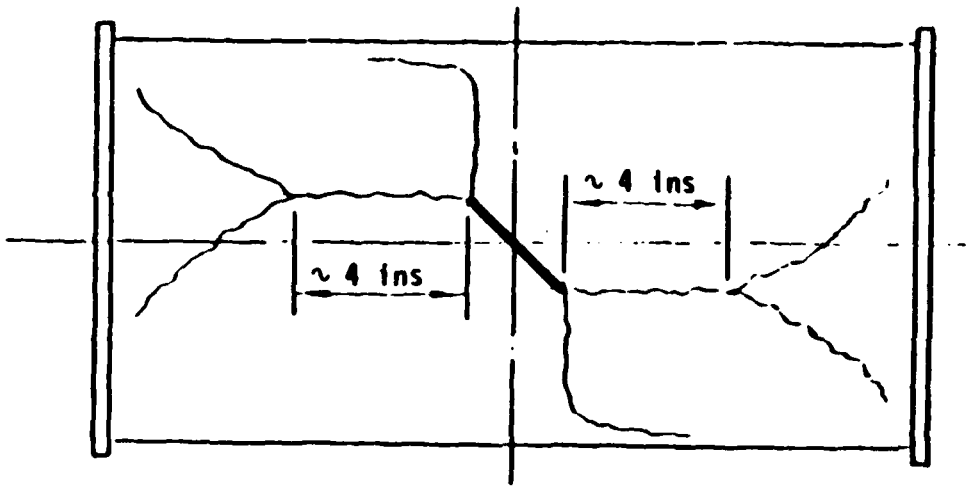

FIGURE 17 Failure Mode for Cylinder 106

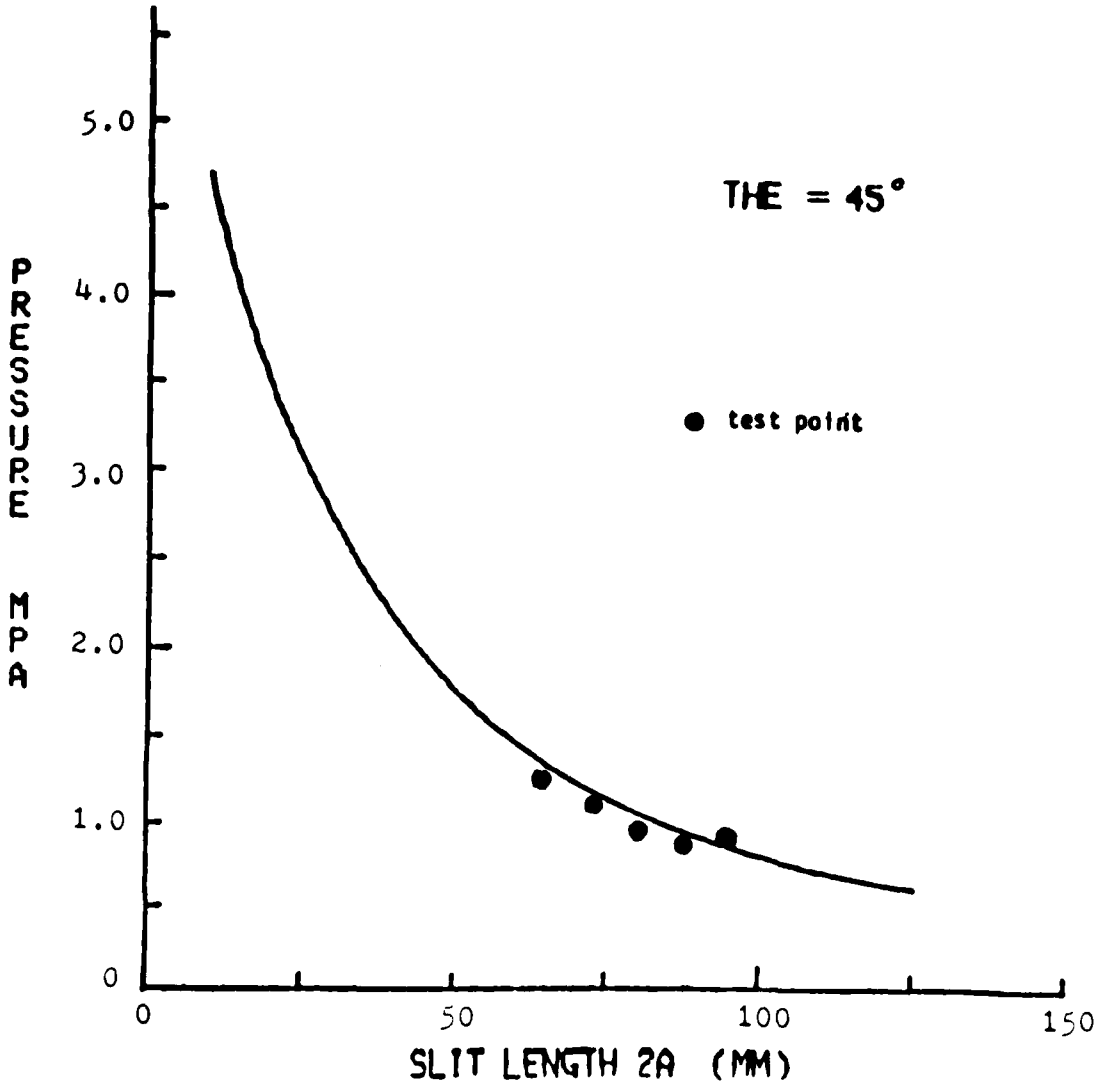

FIGURE 18 Measured and Predicted Failure Pressures for 45 Degree Slits

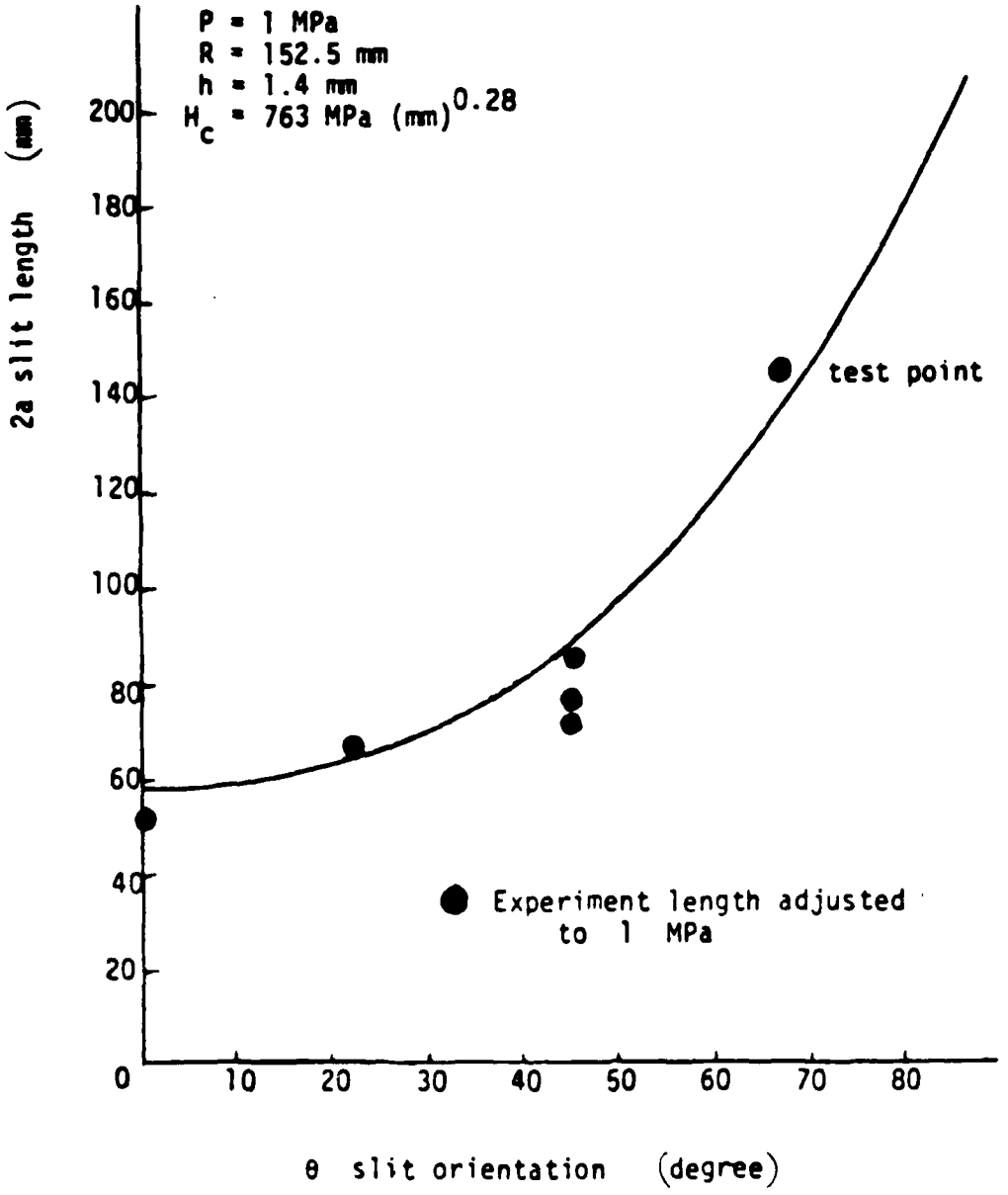

FIGURE 19 Measured and Predicted Slit Lengths Versus Slit Orientation Angle

	Flaws	Note	2c	$\frac{a}{c}$	P_{test} (PSI)	P_{test} (MPa)	K_{two}	P_{two} (MPa)
Tube 5	-	2 (in)		0	145	1.001	2.037*	1.144
Tube 15	- -	2-0.5-2 (in)	2.5	0.8	150	1.034	2.07	1.126
Tube 16	- -	2-1-2 (in)	3	0.666	160	1.103	2.12	1.099
Tube 18	- -	2-0.25-2 (in)	2.25	0.888	105	0.731	2.48	0.940
Tube 20	- -	2-0.125-2 (in)	2.125	0.941	70	0.483	2.67	0.873
Tube 21	- -	2-2-2 (in)	4	0.5	140	0.966	2.18	1.069

*K_{slit}

Test results for specimens with colinear slits

FIGURE 20 Test Results for Cylinders with Colinear Slits

1	2	3	4	5	6	7	8	9
No	Flaw	Note	p_{test} (PSI)	p_{test} (MPa)	p_{hole} (MPa)	p_{slit} (MPa)		K_{hole}
Tube 17		D = 2 (in)	170	1.172	1.114	1.144	3.151	2.037
Tube 23		D = 2 (in)	165	1.138	1.114	1.144	3.151	2.037
Tube 26		D = 3 (in)	120	0.826	0.828	0.732	4.726	2.514
Tube 27		D = 2.5 (in)	150	1.034	0.928	0.903	3.937	2.365

Test results of cylinders with circular holes

FIGURE 21 Test Results for Cylinder with Circular Holes

1	2	3	4	5	6	7
No	Flaw	Note (in x in)	p_{test} (PSI)	p_{test} (MPa)	p_{long} (MPa)	K_{long}
Tube 14		2 x 0.5	185	1.275	1.144	2.037
Tube 19		2 x 1	189	1.303	1.144	2.037
Tube 22		2.5 x 2	150	1.034	0.928	2.365

Test results of cylinders with long holes

FIGURE 22 Test Results for Cylinders with Long Holes

	Flaw	Notes	P_{test} (MPa)	P_{test} (PSI)	P_{plus} (MPa)	K_{plus}
Tube T5	-	L-2 ins	1.001	145	1.144	2.037
Tube 13	-0-	D=0.25 in L=2ins	1.083	157	1.144	2.037
Tube 24	-0-	D-1 in L=2 ins	1.034	150	1.144	2.037
Tube 25	-0-	D=1.5 ins L-2 ins	1.103	160	1.144	2.037

Test results of cylinders with holes and slits

FIGURE 23 Test Results for Cylinders with Holes and Slits

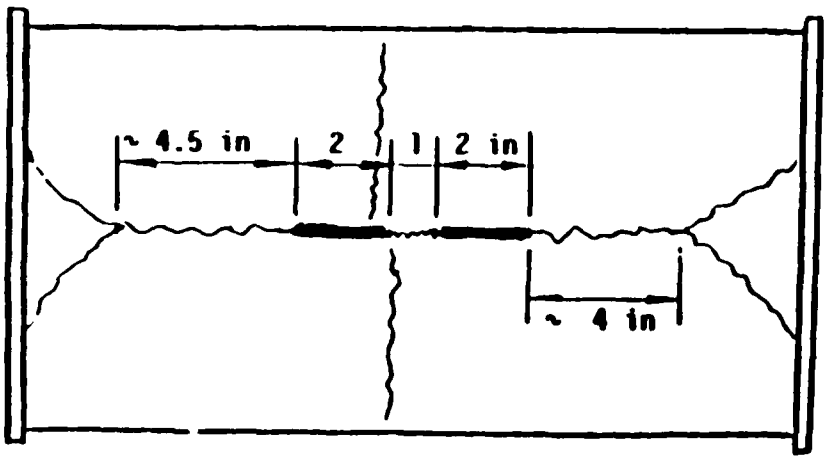

FIGURE 24 Failure Mode for Cylinder 16

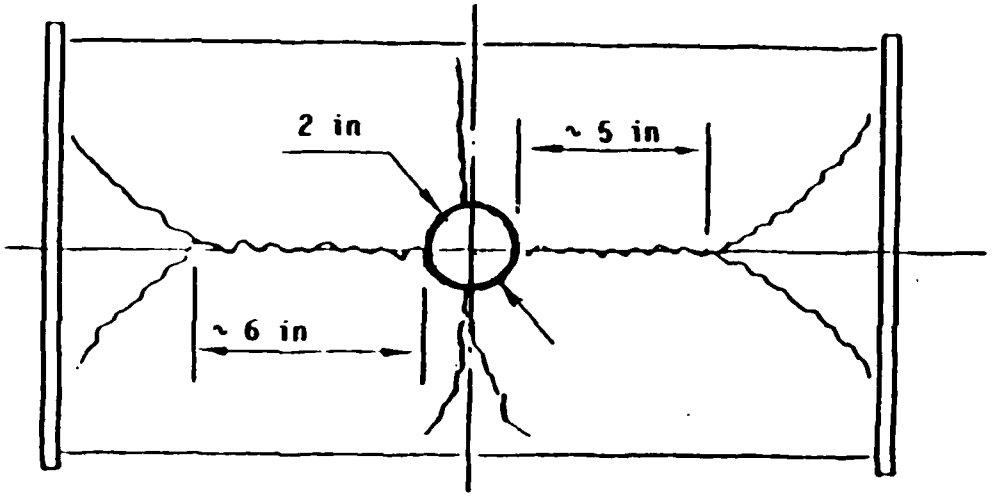

FIGURE 25 *Failure Mode for Cylinder 27*

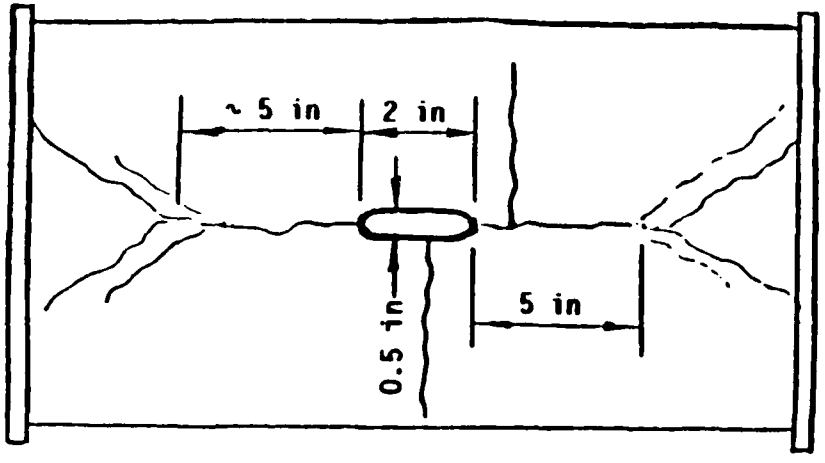

FIGURE 26 Failure Mode for Cylinder 14

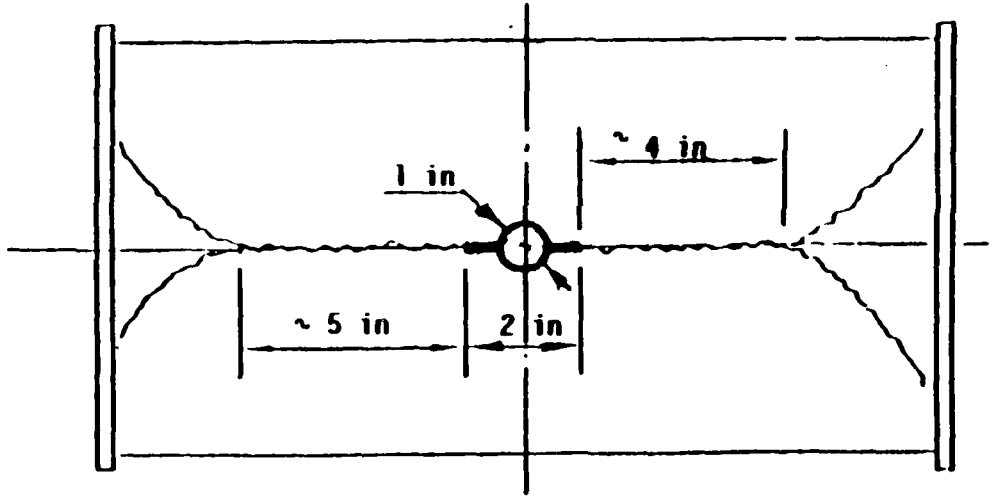

FIGURE 27 Failure Mode for Cylinder 24

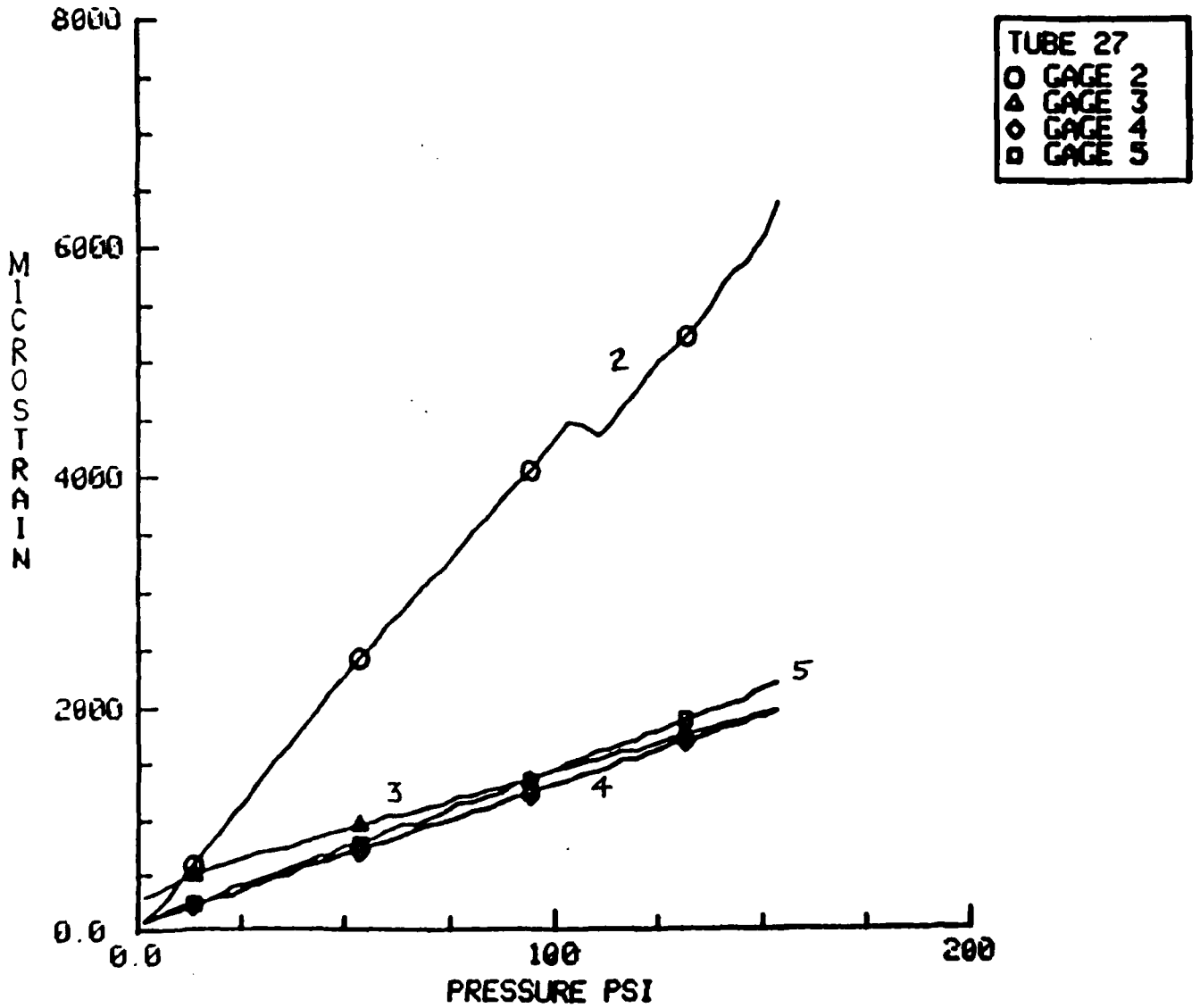

FIGURE 28 Measured Hoop Strains at Various Locations for Cylinder 27

△ test data for D = 2 in
x test data for D = 2.5 in
C test data for D = 3 in

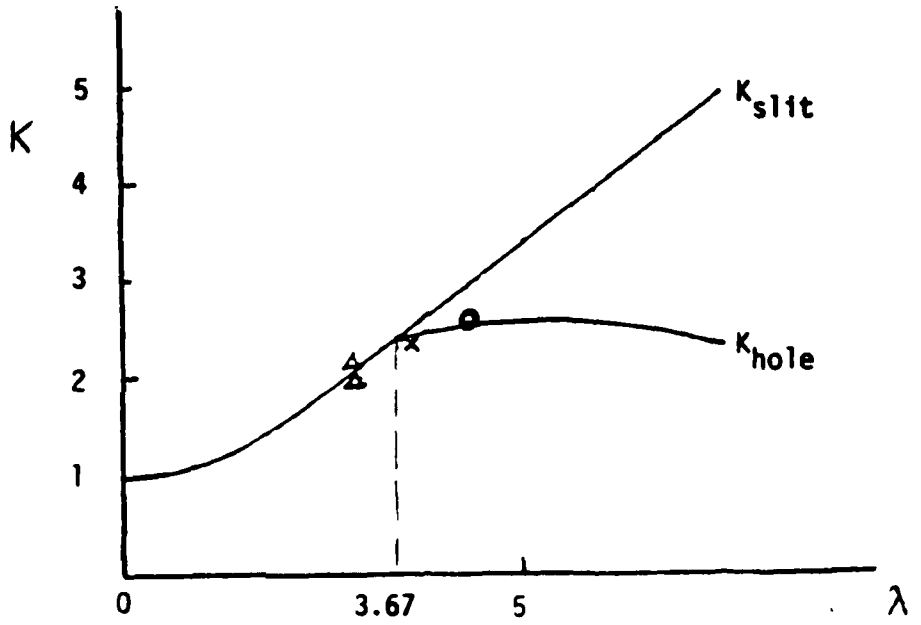

FIGURE 29 Stress Concentration Factor K for a Circular Hole

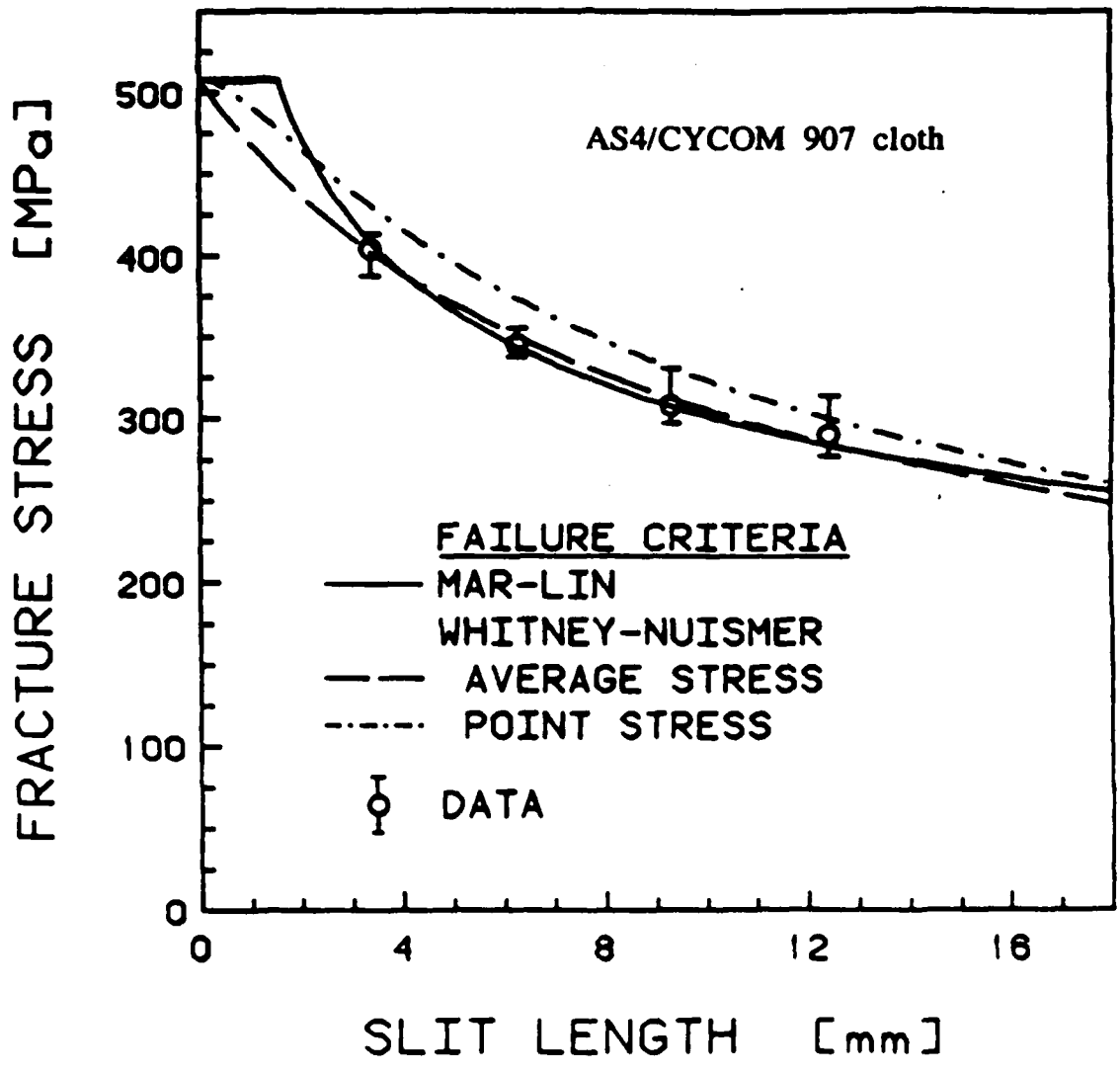

FIGURE 30 Fracture Stresses for $(0, 45)_s$ Flat Coupons with Slits

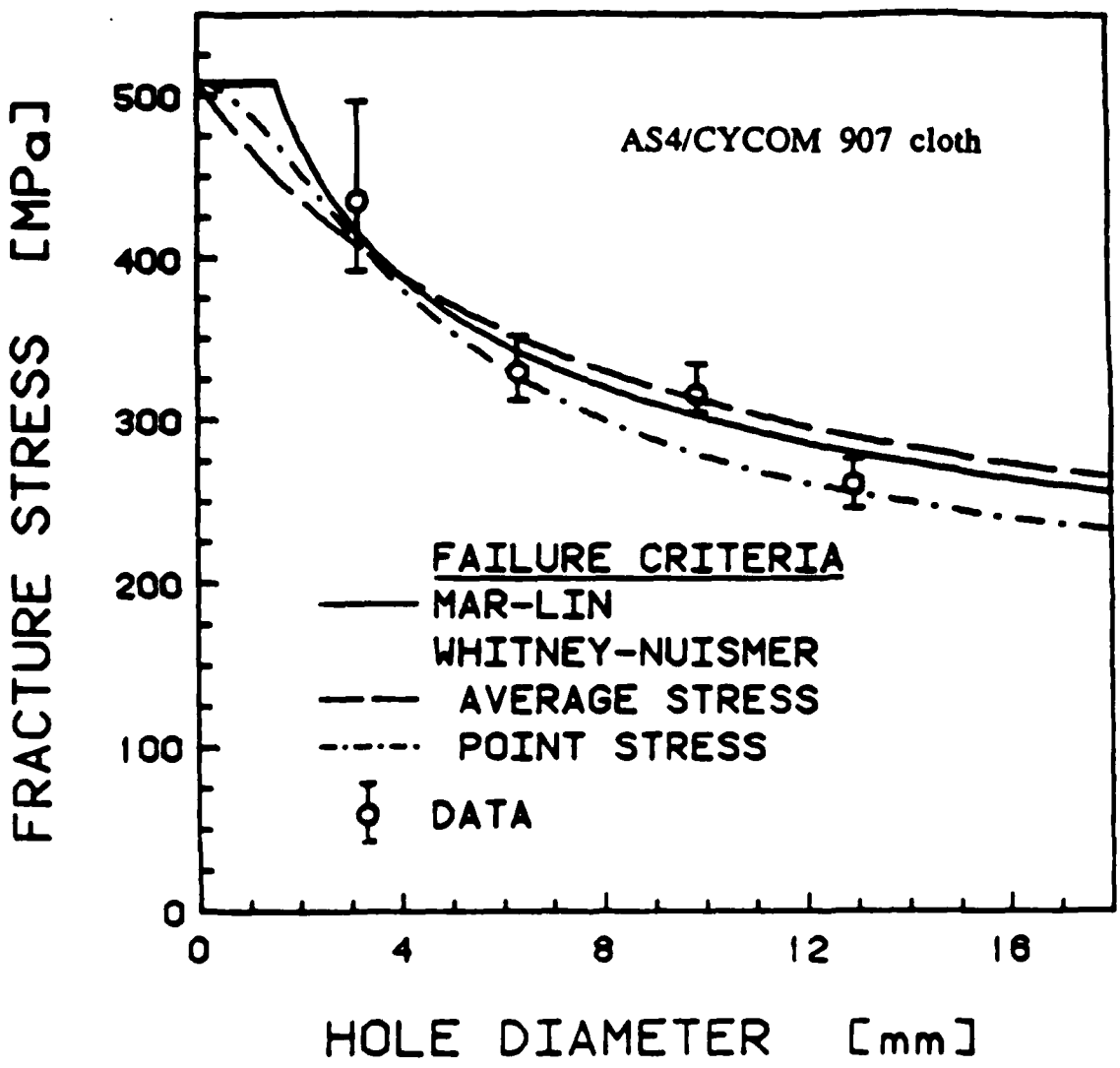

FIGURE 31 Fracture Stresses for $(0, 45)_s$ Flat Coupons with Holes

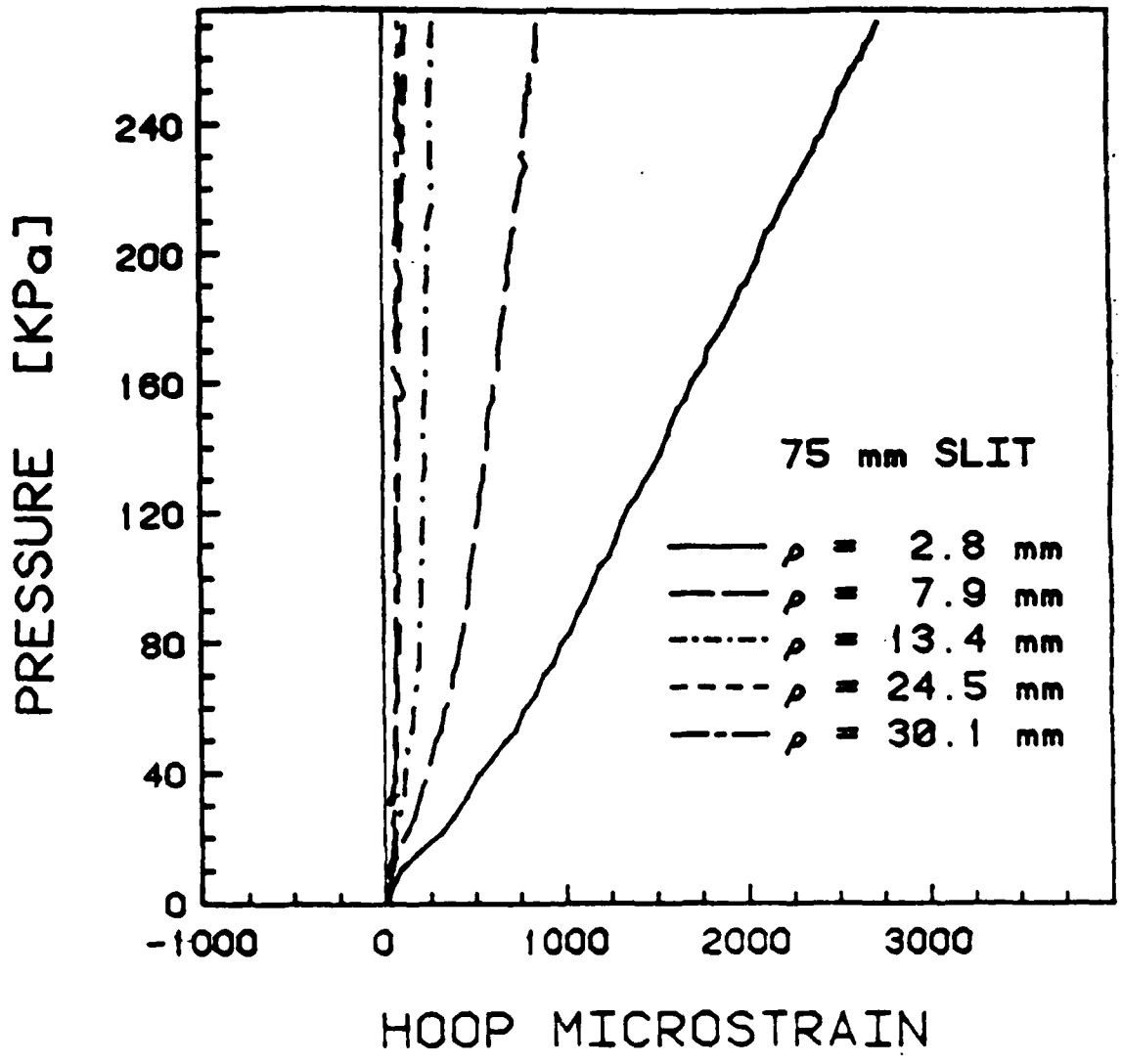

FIGURE 32 Measured Hoop Strains at Various Locations for Cylinder with a 75 mm Slit

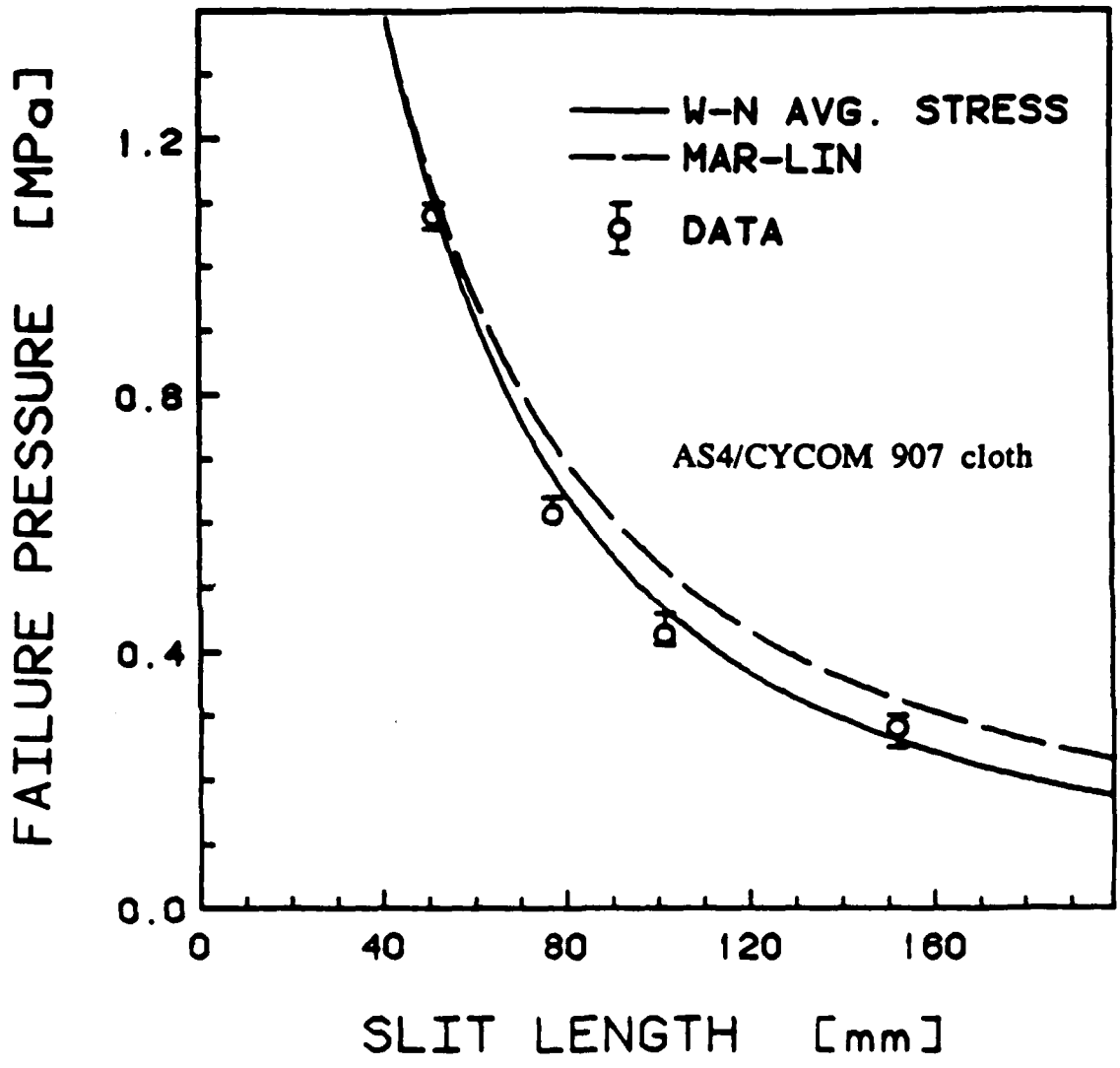

FIGURE 33 Measured and Predicted Failure Pressures for Cylinders with Slits

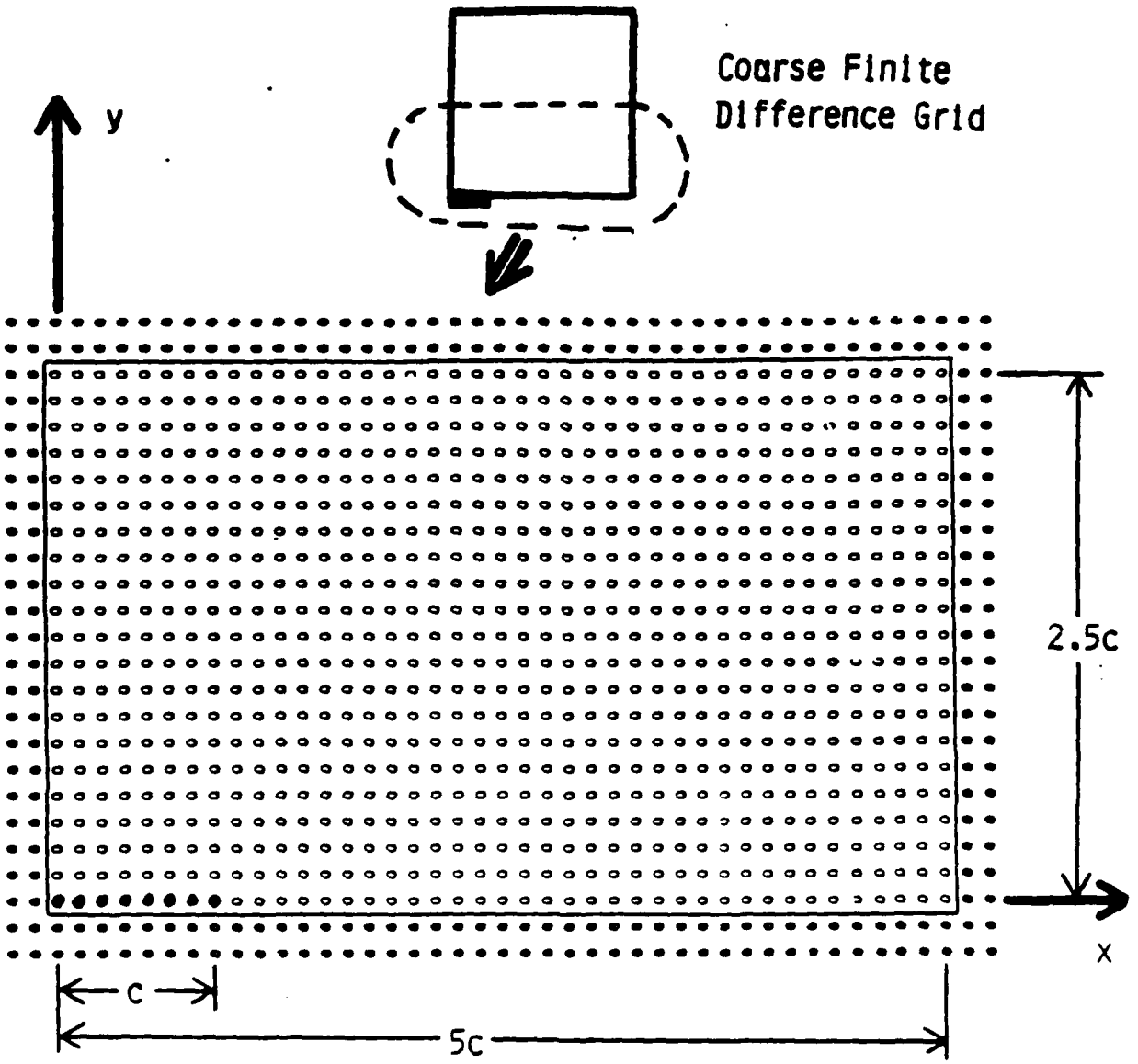

- Normal Node
- Crack Node
- Imaginary Node

FIGURE 34 Refined Finite Difference Grid Used in Analysis

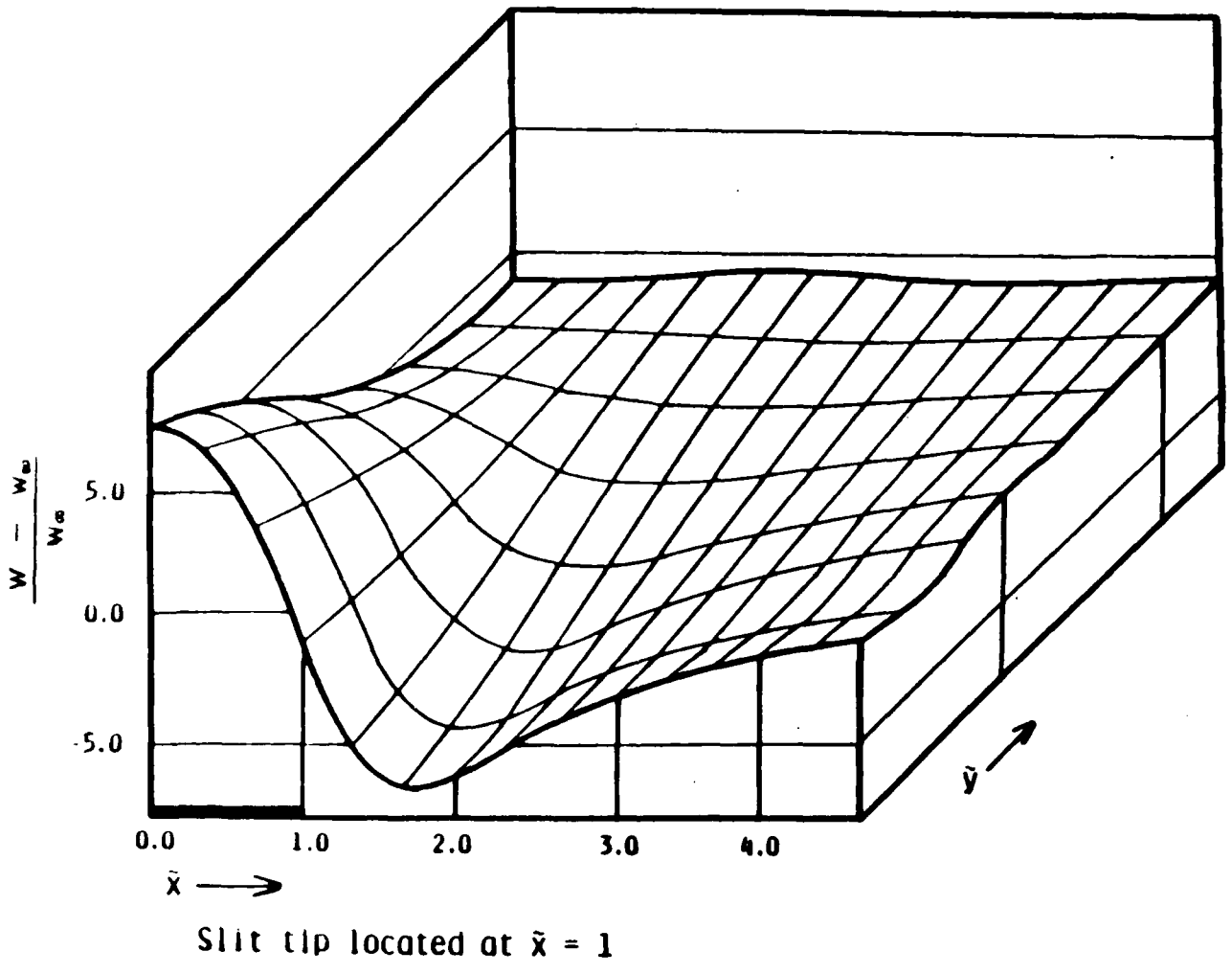

FIGURE 35 Analytical Displacements w Obtained from Finite Difference Analysis, 75 mm Slit

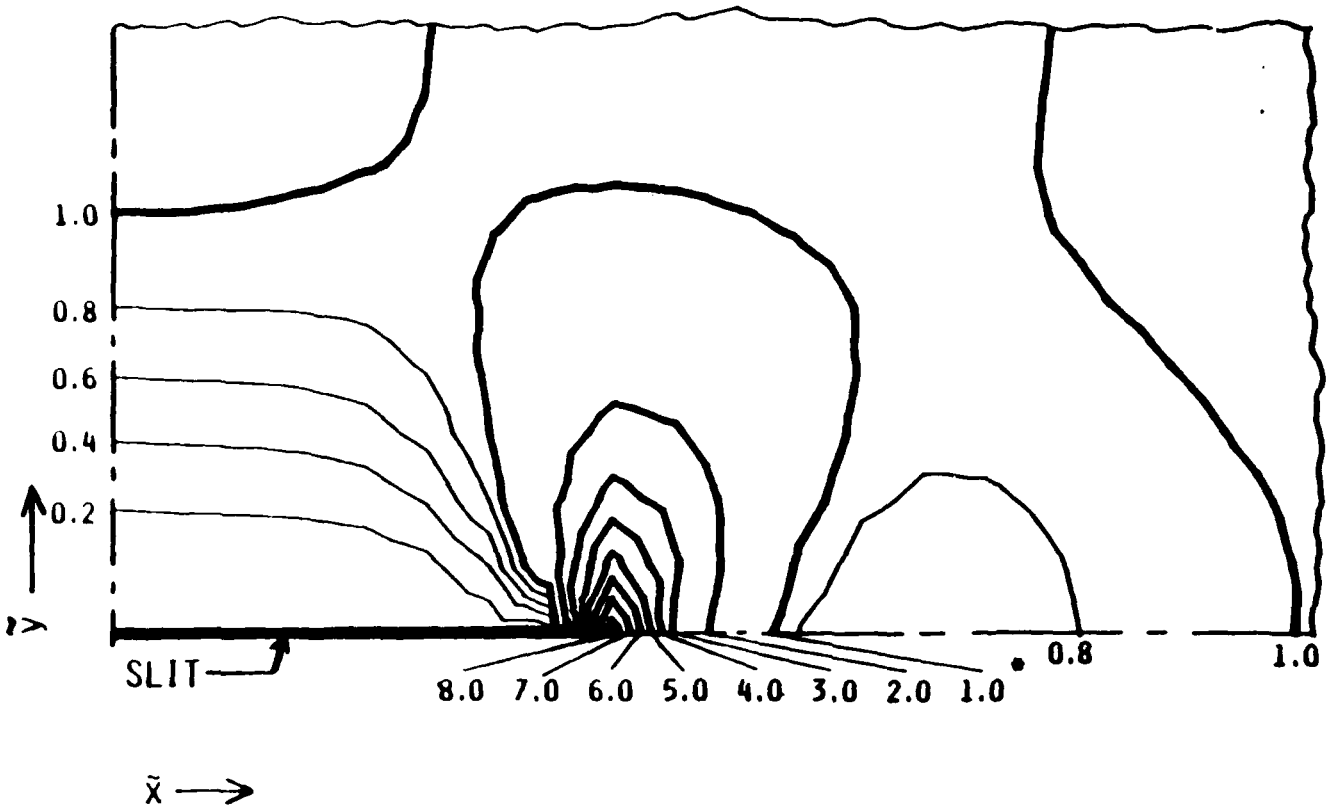

FIGURE 36 Hoop Stress Concentration Factor K Obtained from Finite Difference Analysis, 75 mm Slit

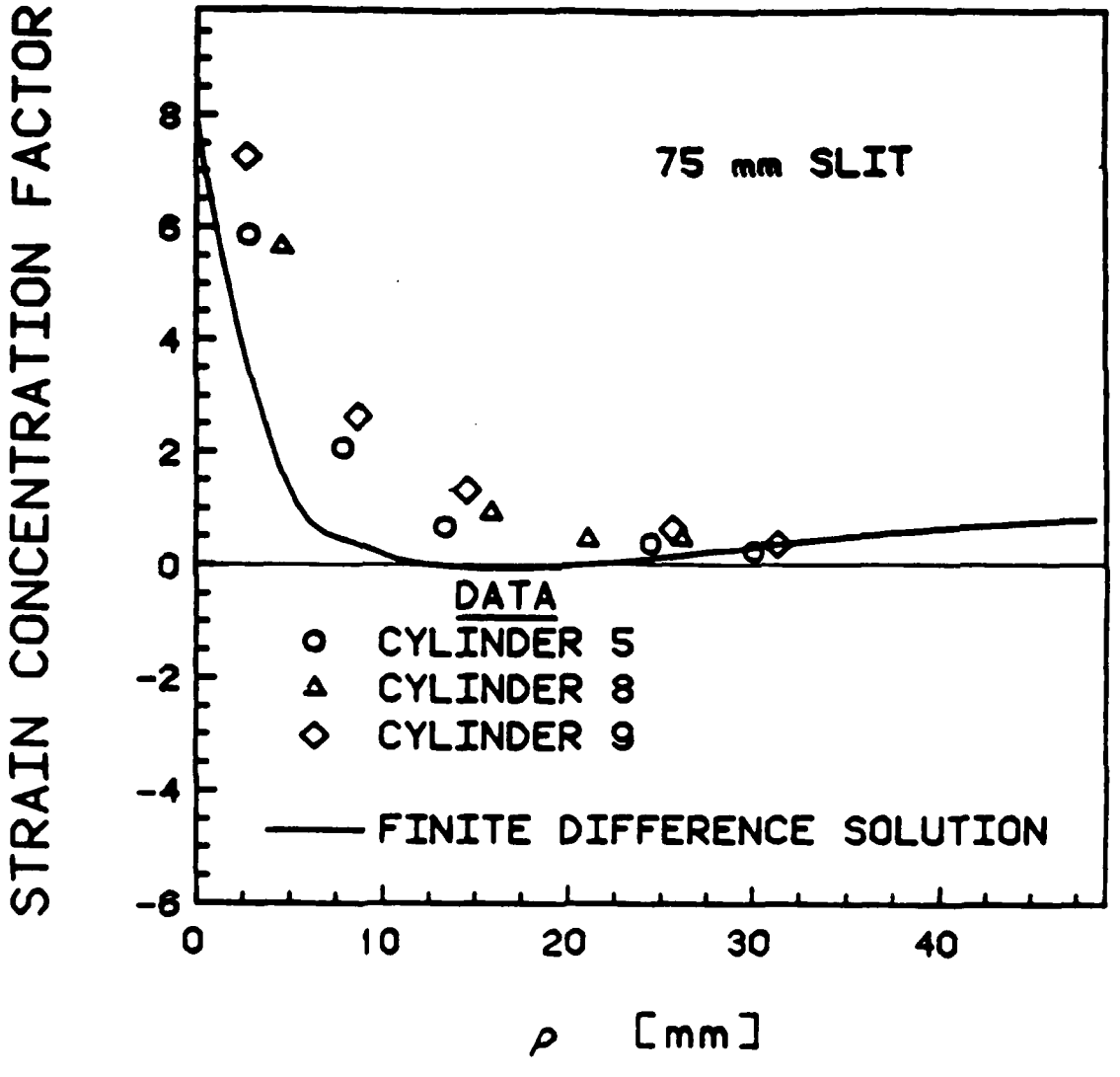

FIGURE 37 Measured and Predicted Hoop Strains for Cylinder with a 75 mm Slit

U.S. Government Printing Office: 1987 — 748-091/60969

END

9-87

DTIC